

~~CONFIDENTIAL~~Copy 308
RM E52C21

NACA RM E52C21

~~53-30-45~~
~~NACA~~TECH LIBRARY KAFB, NM
0143407

RESEARCH MEMORANDUM

EXPERIMENTAL INVESTIGATION OF AIR-COOLED TURBINE

BLADES IN TURBOJET ENGINE

XI - INTERNAL-STRUT-SUPPORTED ROTOR BLADE

By Reeves P. Cochran, Francis S. Stepka, and
Morton H. Krasner

Lewis Flight Propulsion Laboratory

AS. ion (ac. 1 g Cleveland, Ohio. *Unclassified*)Nasa Tech Pbl. Announcement #102
(OFFICIAL AUTHORIZED TO CHANGE)

6;

22 June 56

GRADE Or OFFICER MAKING CHANGE)

5 Apr 61

CLASSIFIED DOCUMENT

This material contains information affecting the National Defense of the United States within the meaning of the espionage laws, Title 18, U.S.C., §§ 793 and 794, the transmission or revelation of its contents in any manner to an unauthorized person is prohibited by law.

NATIONAL ADVISORY COMMITTEE
FOR AERONAUTICS

WASHINGTON

June 2, 1952

219.98/13

~~CONFIDENTIAL~~PERMANENT
RECORD



0143407

1H

NACA RM E52C21

~~CONFIDENTIAL~~

NATIONAL ADVISORY COMMITTEE FOR AERONAUTICS

RESEARCH MEMORANDUM

EXPERIMENTAL INVESTIGATION OF AIR-COOLED TURBINE

BLADES IN TURBOJET ENGINE

XI - INTERNAL-STRUT-SUPPORTED ROTOR BLADE

By Reeves P. Cochran, Francis S. Stepka, and
Morton H. Krasner

SUMMARY

An air-cooled internal-strut-supported blade was investigated in a modified production turbojet engine to determine the cooling effectiveness of this type of blade design and the cooling-air pressure loss through the blade under engine operating conditions. This blade consisted of a finned internal load-carrying member or strut integral with the blade mounting base and an attached shell that forms the airfoil shape and insulates the strut from the direct effects of the hot gas stream. The greater part of the investigation was conducted over a range of engine speeds from 4000 to 11,500 rpm and a range of coolant-to-gas weight-flow ratios per blade from approximately 0.02 to 0.10. The experimental results of this investigation are presented and compared with the results from an analytical investigation of a similar internal-strut-supported blade and with the results of experimental investigations of shell-supported blades.

At operating conditions of rated engine speed, an effective gas temperature of 1450° F, a cooling-air temperature of 450° F, and a coolant-to-gas weight-flow ratio per blade of 0.03, the stress ratio factor (a ratio of the integrated mean of the allowable stress for each radial blade element to the calculated mean centrifugal stress) for the strut-supported blade was 3.06 as compared with 2.51 for an improved shell-supported blade. At these same operating conditions, the temperature of the strut of the strut-supported blade at the 3/8-span midchord location was 728° F and the temperature of the shell of the shell-supported blade at the same location was 1010° F. The strut-supported blade, because of the lower operating temperatures and higher stress-ratio factors, indicates promise of operating at higher turbine-inlet temperatures or at lower coolant-to-gas weight-flow ratios per blade than the shell-supported blade.

~~CONFIDENTIAL~~

2501

The pressure losses through the strut-supported blade are within the range of losses obtained with previously investigated shell-supported blades; however, the cooling effectiveness of the strut-supported blade is higher, for a given pressure loss, than the cooling effectiveness of any of the shell-supported blades previously investigated. Comparisons of the analytically calculated and the extrapolated measured average strut temperatures showed that, at an effective gas temperature of 1530°F , a cooling-air temperature of 200°F , and for coolant-to-gas weight-flow ratios per blade up to 0.02, the extrapolated measured temperature was a maximum of 60°F higher than the analytically calculated temperature. The analytical method of predicting temperatures in a strut-supported blade was therefore concluded to be sufficiently accurate for design purposes.

INTRODUCTION

An investigation of various air-cooled turbine blade configurations under conditions of actual engine operation is being conducted at the NACA Lewis laboratory in order to determine air-cooled blade designs that will permit the use of noncritical materials both at current turbine-inlet temperatures and at higher turbine-inlet temperatures. Previous investigations of a variety of air-cooled rotor blades (references 1 to 9) have indicated that shell-supported blades of low alloy steels with tubes in the coolant cavity to augment the internal heat-transfer surface area appear to be structurally satisfactory for cooling-air to combustion-gas weight-flow ratios (herein called coolant-to-gas weight-flow ratios) as low as 0.03 when operated in turbojet engines at current turbine-inlet temperatures. Modifications of air-cooled turbine blades to reduce chordwise temperature gradients by conduction or film cooling showed little promise of improving the over-all blade cooling effectiveness; consequently, other means of improving air-cooled blades were studied. A promising concept of blade design was derived from this study that indicated potentialities for operation at higher gas temperatures and at lower coolant-flow requirements than obtainable with previously investigated blades. The proposed blade design uses a cooled internal element or strut as the main support member thereby taking advantage of the lower temperature level and correspondingly higher permissible stress level in the internal strut. The blade shell is attached to the strut in such a manner that the shell is required to support its own weight only between points of attachment. An analytical comparison of this internal-strut-supported blade with a shell-supported blade at an effective gas temperature of 1530°F and a coolant-to-gas weight-flow ratio of 0.02 (reference 10) indicated that the main support member of the internal-strut-supported blade would operate approximately 245°F cooler at the 3/8-span position than the main support member of the shell-supported blade at a similar location, thereby showing a greater potential of the strut-supported blade for

2501 application in turbines with higher gas temperatures. Because of the great improvements in cooling effectiveness indicated in reference 10, an internal-strut-supported blade was fabricated and investigated in a modified turbojet engine in order (1) to determine the cooling effectiveness and the cooling-air pressure losses of the strut-supported blade, and (2) to compare the experimental results of this investigation with experimental results of previously investigated air-cooled blades and with results obtained in the analytical investigation of a similar strut-supported blade in reference 10. The results of this investigation were used to compare the strength-carrying capacity of the strut-supported blade with that of a shell-supported blade, and to evaluate the possibility of operating a strut-supported blade at either higher turbine-inlet temperatures or lower coolant flows than shell-supported blades or both. Blade temperatures were investigated over a range of engine speeds from 4000 to 11,500 rpm, and the cooling-air pressure losses were investigated over a range of engine speeds from 4000 to 10,000 rpm. The greater part of both of these investigations was conducted over a range of coolant-to-gas weight-flow ratios per blade from approximately 0.02 to 0.10.

APPARATUS

Engine

The modified turbojet engine and the engine instrumentation used for this investigation are described in detail in references 1 and 2. There was only one experimental cooled internal-strut-supported blade in this investigation and it was balanced in the turbine wheel by a shortened solid blade of equivalent weight installed diametrically opposite. For part of the investigation, a hollow uncooled blade of the same profile as the experimental blade was installed on each side of the experimental blade to provide more favorable flow conditions around the blade. A similar blade on either side of the shortened solid blade was used for balance of the wheel. For the remainder of the investigation, conventional uncooled turbine blades were used in the positions adjacent to the cooled blade.

Blade Design and Fabrication

Blade design. - The basic principle of the air-cooled, internal-strut-supported blade design is the thermal isolation of the load-carrying member from the hot gas stream. This isolation is accomplished by attaching a thin airfoil-shaped, sheetmetal shell to projections on the strut at several points and by passing cooling air between the shell and the strut. In such a design the strut must carry the entire weight of the shell in addition to its own weight. It was pointed out in reference 10 that the best way to support this load was to distribute

~~CONFIDENTIAL~~

it over the whole span of the blade. Because of the added weight of the shell, the stresses in the root of the strut will be higher than in the more conventional shell-supported blades unless a greater taper ratio can be built into the strut. The disadvantage of the higher stress level in the strut can be more than offset, however, by the fact that the strut operates at a much lower temperature than the shell of the shell-supported blades and can, therefore, safely permit high stress levels. Factors affecting the maximum taper in the strut are the taper in the airfoil, the cooling-air flow-area requirements at the root section of the blade, and the need for projections or fins on the strut to provide points of attachment for the shell and to provide passages for the cooling air all the way to the tip section. A tapered airfoil would increase the possibilities for a more favorable taper ratio in the strut, but in the present investigation the airfoil was untapered and nontwisted so that heat-transfer results could be compared with similar results obtained on previously investigated blades reported in references 1 to 9. Additional cooling fins on the strut, which are not in contact with the shell, help to reduce the strut temperatures. Tapering these attachment and cooling fins would help to reduce the root stresses on the strut, but because of the difficulties in fabricating tapered fins untapered fins were used in this experimental blade.

Because of the nature of the test apparatus available for this investigation, it was necessary that the blade have a serrated mounting base and that the cooling air be introduced through the blade base. In order to meet these requirements, the strut had to be supported on the base in such a manner that the cooling air could pass through the blade base to reach both sides of the blade shell.

In view of the previously mentioned requirements and desirable features for an internal-strut-supported blade, the blade shown in figures 1 and 2 was designed for use in this investigation. The strut and shell are shown before assembly in figure 1(a) and after assembly, in figure 1(b). A chordwise cross-sectional view of the blade profile at the root appears in figure 2(a). The outside profile of the shell is the same as that of configuration A of reference 9 and is similar to the root-section profile of the turbine-rotor blade for the engine in which this investigation was conducted. A spanwise cross-sectional view of the blade appears in figure 2(b). Cooling air, which is introduced at the base of the blade, flows radially outward between the fins on the strut and is discharged at the blade tip. Thus, the strut is surrounded by cooling air except along the edges of the fins in contact with the shell. In addition, the inside surface of the shell is cooled by the air flowing past.

The main body of the strut is tapered spanwise from a midchord thickness of 0.20 inch at the root section to a midchord thickness of 0.04 inch at the 3/4-span section where it ends. Integral with the main

body of the strut are a total of 38 parallel radial fins distributed chordwise along both sides of the blade as shown in figures 2 and 3. Fourteen of these fins are 0.040-inch thick and are in contact with the blade shell for their entire length. Twelve of these fins extend the full span of the blade. At the $3/4$ span, the strut ends and the 12 fins combine in pairs to form 6 fins extending from the suction to the pressure side of the blade. The remaining two fins, located in the trailing edge, extend only to the $3/4$ -span section. The shell is attached to the strut on the edges of these fins. The remaining 24 fins, which are 0.020-inch thick and extend from the root to the $3/4$ -span section, do not touch the shell except for a $1/4$ -inch length at the $3/4$ -span position. These fins serve only to increase the heat-transfer surface of the strut.

A chordwise slot on each side of the blade base introduces cooling air from the supply tube in the wheel through the blade base to a plenum chamber in the top of the base platform. This chamber aids in the distribution of the cooling air to all parts of the blade. The top of this chamber is covered by a cooling cap (fig. 2(b)) which is welded to the blade base and to the blade shell at the root section.

This blade was of the same general design as the blade analytically developed in reference 10.

Shell attachment. - One of the problems associated with the strut-supported blade design was that of attaching and supporting the hot shell on a cool internal member. The points of attachment between the shell and strut had to be sufficiently strong in order to transfer the load of the shell to the strut. However, because these points of attachment were also paths of heat conduction into the strut, the contact area had to be as small as possible to minimize heat transfer to the supporting strut. The most expedient method of fulfilling the requirements of this attachment problem was spot-welding intermittently along the span.

The spot welds are subjected to thermal loads because of the temperature gradient between the strut and shell as well as the centrifugal load of the shell. Therefore, a calculation was made to determine the magnitude of these loads assuming 14 chordwise rows of spot welds along the span as shown in figure 2(b). These rows are numbered consecutively from row 1 near the root to row 14 near the tip. The simulated operating conditions for this calculation were rated engine speed (11,500 rpm) and gas shell and strut temperature distributions as shown in figure 6 of reference 10. The details of the method of calculating the thermal forces are given in appendix A. The first calculations were made for 14 spot welds per row except for rows 12 to 14 in which there were 12 welds per row, giving a total of 190 spot welds on the entire blade.

The calculation showed that the maximum thermal force occurred at the row nearest the tip and was 70 pounds per spot weld. With the assumption that each row of spot welds carries a strip of shell 1 inches wide, the center of gravity of which is at the same radial position as the row of spot welds, the maximum calculated centrifugal load per spot weld, which also occurred in the row nearest the tip, was 28 pounds. Therefore, the maximum total load on a spot weld was 98 pounds and occurred in the row of welds nearest the tip of the blade.

In order to judge the adequacy of the spot welds under such loads, an experimental investigation was made of the strength of the spot welds joining samples of the strut and shell materials in an arrangement similar to that found in the blade. The best results from the standpoint of maximum strength and minimum dimpling of the shell were obtained with an electrode diameter of 1/32 inch, a welding force of 15 pounds, and a welding machine setting for high current flow. Shear-strength values obtained with this technique ranged from 100 to 175 pounds per spot weld at room temperature and from 95 to 120 pounds per spot weld at 1000° F.

These results indicated that the last row of spot welds under a calculated shear load of 98 pounds would be operating very close to the stress level at which failure would occur. Because this row was assumed to contain only 12 spot welds the occurrence of a faulty weld might have caused failure of the row and subsequent progressive failure of the spot welds all the way down the blade. In order to avoid this, the number of spot welds at the eleventh row was increased to 38 by spot-welding to the 0.020-inch thick fins as well as to the 0.040-inch fins (see fig. 1(b)). A calculation was then made assuming failure of all the spot welds in rows 12 to 14. This resulted in a total shear force of 65 pounds per spot weld in row 11. This maximum value of load on the spot welds was considered safe particularly with respect to the greater number of spot welds in the row exposed to the load. Additional calculations showed that the shell could support its own weight from row 11 outward.

As a result of the experimental strength investigation and the analytical stress calculations on the attachment of the shell to the fins of the strut with spot welds, a final spot-weld pattern consisting of 14 chordwise rows with 14 spot welds per row in rows 1 to 10, 38 spot welds in row 11, and 12 spot welds per row in rows 12 to 14, or a total of 214 spot welds on the entire blade, was evolved for use in fabricating the internal-strut-supported blade. Some simplified models of the airfoil portion of the strut were fitted with shells by use of this spot-weld pattern and the assemblies were investigated statically under conditions of temperature difference between shell and strut in order to determine the strength of the shell attachment under simulated thermal loads. The results of this investigation indicated that large temperature gradients caused failures of a few spot welds in the last

one-quarter span, as had been anticipated, but in the remainder of the blade the spot welds held successfully. Centrifugal forces due to rotation would increase the possibility of spot-weld failure, but because these forces are small in comparison with the thermal forces, spot welding in the manner previously specified was concluded to be satisfactory for attaching the shell to the strut.

Fabrication. - The fabrication of this blade was accomplished in an experimental manner and not by methods that would ordinarily be used in production. This type of blade, however, should easily lend itself to a number of conventional production-fabrication techniques such as casting the integral strut-base section or by brazing spanwise laminations to form the strut-base section. Further development of the basic design, however, will be necessary before this blade could be reproduced in production quantities by economical methods.

In making this blade, the strut and base were machined integrally from a bar of SAE 4340 steel, a material with about 3 percent critical metal content. Timken 17-22A(S) alloy steel would be a better material for the strut with respect to strength at high temperature, but because of the unavailability of this material, SAE 4340 steel was used for this experimental blade. The profile of the inner surface of the shell was cut on the bar and the fins were formed by milling parallel spanwise grooves of varying depths from the root section to the 3/4-span section. A depression was machined in the top of the base and the two cooling-air slots were cut in the base to form the cavity for the blade-base plenum chamber and the cooling-air entrance through the base, as shown in figure 2(b). The strut and rough-machined base were then heat-treated to a hardness of Rockwell C-25.

The shell was made of a 0.018-inch thick Inconel sheet that was rolled into a tube, filled with wax, and die formed to the proper profile similar to the method described in reference 11. The cooling cap was cut from 0.060-inch Inconel sheet to the size of the blade base platform with a cutout the shape of the shell profile. The shell and the cooling cap were welded together, and the shell, but not the cooling cap, was then split spanwise at the leading and trailing edges so that it could be welded to the strut at these points. The cooling cap and shell were slipped over the strut and the shell was spot-welded to the strut in the manner described in the previous section of the report. The leading and trailing edges of the shell were then heliarc welded to the strut, and the cooling cap was welded to the top of the blade base in a similar manner. The final step in the fabrication of the blade was the grinding of the base mounting serrations in order to permit installation in the modified turbine rotor.

Blade Instrumentation

Thermocouples for measuring the temperature of the strut at various spanwise and chordwise stations were installed as shown in figure 3 after machining was completed and before assembly was begun. A schematic sketch of the blade and the thermocouple locations is shown in figure 4. An attempt was made to measure a spot-weld temperature and a shell temperature with thermocouples 1 and 2, respectively, at approximately the 3/8-span midchord position on the suction side. These two thermocouples failed early in the test running, however, and no temperatures were recorded for these locations. Thermocouple 3 was located on the suction side of the strut at the 1/4-chord, 3/4-span position in order to measure the temperature of the main body of the strut at this point. Thermocouples 4 to 6 were installed from the pressure side of the support member, but the thermocouple junctions were located so as to measure the temperatures at the base of the 0.040-inch thick fins of the strut on the suction side. They were placed at the leading edge, midchord, and near the trailing edge, respectively, at about 3/8-span from the root.

In addition to the instrumentation on the test blade, thermocouples were installed at approximately the 3/8-span position at the leading edge on two solid uncooled blades in order to measure the effective gas temperature. The temperature of the cooling air at the entrance to the blade base was measured by a thermocouple in the air-supply tube at this point (fig. 4). Details of the rotating thermocouple lead system are described in reference 1.

PROCEDURE

Experimental Procedure

The procedure followed in conducting the experimental runs on the internal-strut-supported blade in engine operation was the same as that followed in previous investigations of other blade configurations (references 1 to 7 and 9). Runs at engine speeds from 4000 to 10,000 rpm were made with the internal-strut-supported blade as previously described. The failure of an uncooled hollow blade adjacent to the strut-supported blade at an engine speed of 11,500 rpm damaged the strut-supported blade to the extent that approximately 1 inch of the span had to be removed at the tip. After replacing the hollow uncooled blades with conventional twisted solid blades, the investigation was continued with the shortened test blade and runs were made over a range of engine speeds from 4000 to 11,500 rpm. At each engine speed, the cooling-air flow, which was supplied from an external source, was varied, for the greater portion of the investigation, over a range of coolant-to-gas weight-flow ratios

per blade from approximately 0.02 to 0.10. The investigation was conducted with an adjustable exhaust nozzle in the full-open position which gave effective temperatures lower than the temperatures that would exist at rated engine thrust.

Calculation Procedure

Blade-temperature correlation. - It has been shown in reference 1 that the relation $\phi = \frac{T_{g,e} - T_B}{T_{g,e} - T_{a,e,h}}$ is approximately a function of cooling-air and combustion-gas weight flows for hollow air-cooled blades, blades with inserts, and blades with internal fins. (All symbols used in this report are given in appendix B.) In this expression, T_B is the local temperature of the blade shell, $T_{a,e,h}$ is the cooling-air temperature at the root of the blade, and $T_{g,e}$ is the local effective gas temperature.

Unpublished numerical examples using the analysis of reference 10 showed that, when ϕ for the strut was computed using the strut temperature for T_B , only slight variations in the calculated values of ϕ for a specific spanwise position were encountered when the values of cooling-air temperature at the blade root $T_{a,e,h}$ and local effective gas temperature were changed arbitrarily and cooling-air and combustion-gas weight flows remained constant. These numerical examples indicated that for strut-supported blades, ϕ was approximately a function of cooling-air weight flow w_a and combustion-gas weight flow w_g as in the case of the blade configurations of previous investigations of this series. Because $1-\phi$ is more suitable than ϕ for plotting on logarithmic scales where the blade cooling effectiveness is high, the data were correlated by a plot of $1-\phi$ against w_a/w_g .

Method of obtaining data at rated engine speed. - In order to determine values of $1-\phi$ for the full-length blade at rated engine speed (11,500 rpm), the values of $1-\phi$ for this blade at combustion-gas flows corresponding to lower speeds (4000 to 10,000 rpm) were compared with the values of $1-\phi$ for the shortened blade at combustion-gas flows corresponding to the entire range of engine speeds from 4000 to 11,500 rpm at a number of coolant-to-gas weight-flow ratios per blade. The curves of $1-\phi$ for the full-length blade were extrapolated to the combustion-gas flow of rated speed by extending the curves for the full-length blade at the same slope as the corresponding curves for the shortened blade.

Pressure loss through blade. - A method of correlating the cooling-air pressure loss from the rotor hub to the blade tip that occurs when cooling air passes through the rotating coolant passages is developed in reference 2. The value of the pressure-loss parameter

$$Y = \frac{\rho_{a,H,r}}{\rho_0} \left[P'_{a,H,r} - \left(P'_{m,r} - \frac{\eta \omega^2 r_T^2 \rho_{a,H,r}}{70.7} \right) \right] \quad (1)$$

which is obtained for various cooling-air flows and engine speeds is plotted against cooling-air flow. In order to determine the pressure loss through the blade only, the cooling-air pressure loss from rotor hub to the blade base (as determined by static investigation, reference 3) is subtracted from the pressure-loss parameter, so that the pressure loss through the blade then becomes,

$$Y_1 = \frac{\rho_{a,H,r}}{\rho_0} \left[P'_{a,H,r} - \left(P'_{m,r} - \frac{\eta \omega^2 r_T^2 \rho_{a,H,r}}{70.7} \right) \right] - \frac{\rho_{a,H,s}}{\rho_0} \left[P'_{a,H,s} - P_{a,h,s} \right] \quad (2)$$

Equation (2) has been altered from its presentations in references 3 to 7 in order to define some of the variables more fully and to avoid errors in the interpretation of the equation. The subscript *r* refers to pressures and densities measured during engine operation with the turbine rotating. The subscript *s* refers to measurements taken under static conditions.

For very high heat-transfer rates, errors may arise in correlating pressure losses using an inlet density because of the density changes that occur through the passage. For such a case the average density through the passage provides a better correlation. In order to determine if an error was involved in the use of the inlet density rather than an average density in equation (2) for evaluating pressure losses through air-cooled gas-turbine blades, numerical examples were calculated from unpublished pressure-loss data for a blade at static conditions for a wide range of heat-transfer rates using both average and inlet blade densities. The error involved in using the inlet density rather than the average density for purposes of correlation was found to be small; consequently, the use of blade-inlet densities for correlation of cooling-air pressure losses through gas-turbine blades apparently is justified. Numerical examples using a value of $\eta = 0.27$ and pressures obtained from engine data have shown that for all practical

purposes the density ratio $\frac{\rho_{a,H,r}}{\rho_{a,h,r}}$ can be represented as a function

of w_a only. The maximum variation with engine speed for a given value of w_a was approximately ± 2 percent from a mean line through all data for speeds up to 10,000 rpm. Therefore, because it is more convenient to measure the density at the rotor hub than the density at the blade inlet, the pressure losses were correlated by use of equation (2) where the rotor hub density $\rho_{a,H,r}$ was substituted for the blade-inlet density $\rho_{a,h,r}$.

Comparison of cooling effectiveness (for range of coolant flows) of strut-supported blade and shell-supported blade with internal tubes. - In order to obtain the relative temperature level at which the strut-supported blade and a shell-supported blade operate, a comparison was made of the chordwise temperature distributions of the main support members of the strut-supported blade and an improved shell-supported blade (reference 9) that was tube-filled to increase the heat-transfer surface. The comparison of the temperature distributions was made with the data obtained at approximately the 3/8-span positions on both blades. The temperatures of the strut-supported blade were obtained from the blade-temperature data for thermocouple locations 4 to 6 (fig. 4) at an engine speed of 11,500 rpm, a combustion-gas flow of 71.4 pounds per second, and at values of coolant-flow ratios of 0.05 and 0.03. These data were extrapolated by use of the relative temperature ratio $1-\phi$ to conditions of effective gas temperature of 1450° F (at the leading edge) and a cooling-air temperature of 450° F (at the blade root) which would approximately correspond to the temperature of air bled from the outlet of the engine compressor. On the basis of the previously mentioned numerical examples from the data of reference 10, this extrapolation method is considered to give good approximations of blade temperatures under conditions of cooling-air and combustion-gas temperatures other than the actual experimental conditions. This extrapolation method was used throughout the present report.

The temperatures of the shell-supported blade were obtained from the temperature-difference ratios ϕ of reference 9 for five chordwise locations. These data were extrapolated by use of the values $1-\phi$ to the same conditions as the strut-supported blade except that the engine speed was assumed to vary slightly from 11,500 rpm in order to maintain the combustion-gas flow constant at 71.4 pounds per second. This combustion-gas flow did not occur at an engine speed of exactly 11,500 rpm during the investigation of the shell-supported blade because of the difference in the ambient conditions of the two investigations.

In order to compare further the cooling effectiveness of the primary supporting member of the strut-supported blade and the improved shell-supported blade, a comparison was made of the average relative-temperature ratios $1-\phi$ of the two blades at the 3/8-span position

over a range of coolant-to-gas weight-flow ratios per blade at an engine speed of 11,500 rpm. The values of $1-\phi$ for thermocouple positions 4 to 6 were used to determine the average relative-temperature ratio for the strut of the strut-supported blade. The ϕ values at the five chordwise locations previously mentioned in this section for the shell-supported blade were used to determine the average relative-temperature ratio for this blade.

Comparison of stress-ratio factors (for range of coolant flows) of strut-supported blade and shell-supported blade with internal tubes. - In order to evaluate the strut-supported blade on the basis of load-carrying capacity, a comparison was made of the stress-ratio factors (a ratio of the integrated mean of the allowable blade stress for each radial element to the calculated mean centrifugal stress) of the internal-strut-supported blade with an improved shell-supported blade (reference 9), over a range of coolant-to-gas weight-flow ratios per blade.

The stress-ratio factors for the comparisons were calculated in the manner described in reference 9. The temperature data for both blades at rated speed (11,500 rpm), an effective gas temperature of 1450° F, and a cooling-air temperature at the blade base of 450° F were obtained as explained in the previous section. The blades were assumed to be made of Timken 17-22A(S) alloy, a metal with a low critical-material content.

Comparison of cooling effectiveness (for range of pressure losses) of strut-supported and shell-supported blades. - A comparison was made of the cooling effectiveness of the strut-supported blade and two shell-supported blades by using experimental values of the temperature-difference ratio ϕ for the leading edge, trailing edge, and midchord regions at the 3/8-span location for various cooling-air flows which corresponded to given pressure losses through the blades at an engine speed of 10,000 rpm. The two blades chosen for the comparison were a shell-supported blade with 15 fins inserted in the cooling-air passage (reference 2) and a shell-supported, reverse-flow blade (reference 4). The reverse-flow configuration consisted of a tube-filled blade shell that was capped at the tip so that the air that entered the base and flowed through the tube inserts would reverse flow direction at the tip and flow radially inward toward the base and then out of the blade through the spanwise slots at the leading and trailing edges.

The 15-fin blade was chosen for comparison because it had the lowest pressure losses of any of the air-cooled blades previously investigated and represented a desirable goal to attain or exceed with the strut-supported blade. The pressure losses for the reverse-flow blade indicated the level of losses required to obtain effective film-cooling for reduction of chordwise temperature gradients; in addition, the losses for this blade were the maximum for a given air flow for any blade previously investigated.

2501 Comparison of extrapolated experimental and calculated average strut temperatures. - In order to determine the accuracy of the method used in reference 10 to analytically predict temperatures on an internal-strut-supported blade, a comparison of calculated average strut temperatures from figure 7 of reference 10 and average strut temperatures based on extrapolation of the measured values from the present investigation was made at the 3/8-span position for various coolant-to-gas weight-flow ratios per blade. The average relative-temperature ratio 1- ϕ previously discussed was used to extrapolate the experimental temperature data to the conditions of the analytically calculated data ($T_{g,e}$ of 1530° F and $T_{a,e,h}$ of 200° F).

RESULTS AND DISCUSSION

Some representative results of the experimental investigation of the strut-supported blade are shown in figures 5 to 9. Comparisons of these results with those of other blades are shown in figures 10, 11, and 13 to 15. A summary of the engine operating conditions for the full-length strut-supported blade is given in table I and for the shortened blade in table II. The results and comparisons are discussed in the following paragraphs.

Results from Internal-Strut-Supported Blade

Observed temperatures. - The variations of the observed strut temperatures of the full-length internal-strut-supported blade at four thermocouple locations are given in figure 5 for a range of coolant-to-gas weight-flow ratios per blade from 0.024 to 0.104 and a constant engine speed of 10,000 rpm, the highest speed at which the full-length blade was operated. As would be expected, the temperatures shown in figure 5 at any thermocouple location decreased with an increase in w_a/w_g , or primarily an increase in w_a (as w_g remains constant at a given engine speed and combustion-air inlet conditions). The diminishing effect of additional cooling-air flow as the quantity of cooling air increases is evident from the decreasing slope of the temperature curves with increasing coolant-to-gas weight-flow ratios per blade.

The variation of cooling-air temperature at the blade root $T_{a,e,h}$ with the coolant-to-gas weight-flow ratio per blade w_a/w_g for an engine speed of 10,000 rpm is also shown on figure 5. The increase in $T_{a,e,h}$ with a decrease in w_a/w_g was due to the fact that the temperature of the rotor, which was essentially constant for a given engine speed, affected the smaller quantities of cooling air more than the larger quantities.

~~CONFIDENTIAL~~

A chordwise temperature variation at the 3/8-span position is obvious from a comparison of the temperature curves for thermocouples 4 to 6 (fig. 5). This variation is better illustrated in figure 6 where strut temperatures at the 3/8-span position are plotted against chord position for various coolant-to-gas weight-flow ratios per blade. The strut temperature at the 3/4-span position is as high or higher than the temperature at the 3/8-span position for a corresponding chord location (reference 10). Therefore, the temperatures of thermocouple 3 at the 3/4-span position are included in figure 6 to indicate the slope of the curve between the leading edge and midchord positions.

Correlation of temperatures. - The strut temperature data for each thermocouple location were reduced to the nondimensional relative temperature ratio $1-\Phi$ and are recorded in tables I and II. A plot of these data for the full-length blade against coolant-to-gas weight-flow ratio per blade (fig. 7) shows a fairly good correlation of the temperature data on this basis with indications of a small but general trend of decreasing values of $1-\Phi$ for the strut with an increase in engine speed.

A plot of $1-\Phi$ at thermocouple positions 4 to 6 on both the full-length blade and the shortened blade against the engine combustion-gas weight flow corresponding to engine speed at a w_a/w_g value of 0.05 (fig. 8) indicates that $1-\Phi$ for the strut of the full-length blade was always lower, for a particular thermocouple position and engine combustion-gas weight flow, than $1-\Phi$ for the strut of the shortened blade. Similar plots at other w_a/w_g values indicated the same trend. The maximum difference in temperature between the shortened and full-length blades at 10,000 rpm was approximately 25° F. This difference may be the result of replacing the nontwisted blades adjacent to the test blade with conventional twisted blades; or shortening the test blade, or may be due to experimental error. However, the curves for the two blades are similar in shape (fig. 8), which indicated that the cooling characteristics of the two blades were similar though at different levels. Therefore, the $1-\Phi$ curves for the full-length blade were extrapolated to the combustion-gas weight-flow corresponding to rated speed (71.4 lb/sec at 11,500 rpm) by comparison with the corresponding curves for the shortened blade.

Pressure drop. - The losses in cooling-air pressure in the strut-supported blade were determined from the correlation method given in reference 2 and described in the PROCEDURE section of the present report. These pressure losses are shown in figure 9 for various cooling-air flows per blade w_a . It is evident from figure 9 that the cooling-air pressure losses rise rapidly with increasing cooling-air flow per blade. This trend is similar to that of previously investigated blades.

2501

Blade structural aspects. - A visual examination of the strut-supported blade after completion of the 10,000 rpm series on the full-length blade showed that six spot welds in the row nearest the tip had failed. Four of these spot welds were on the concave (pressure) surface and the other two on the convex (suction) surface. At the time of this inspection, there was no permanent elongation of the blade, buckling of the shell between spot welds, or visible cracking in the seam welds at the leading and trailing edges or around the base of the blade. Failure of a hollow uncooled blade adjacent to the strut blade at 11,500 rpm caused numerous spot-weld failures on the concave surface of the shell which buckled outward from the impact. However, no further spot-weld failures occurred during the operation of the shortened blade. At the conclusion of the investigation, the shell was pulled off the strut so that the condition of the strut could be examined. No damage to the remaining part of the strut was evident other than oxidation due to moisture condensation. Although the full-length blade was not run at rated engine speed, its performance up to 10,000 rpm indicated that it should be structurally satisfactory at 11,500 rpm. Further investigations will be necessary in order to determine the effects of rapid changes in temperatures on the spot-weld attachments.

Comparisons of Strut-Supported Blade and Shell-Supported Blades

Cooling effectiveness (for range of coolant flows) of strut-supported blade and shell-supported blade with internal tubes. - The improved shell-supported blade with internal tubes (blade 12, reference 9) was selected for comparison with the strut-supported blade on the bases of the chordwise temperature distribution and the average relative temperature ratio because this blade was the most promising of the shell-supported blades previously investigated. The comparisons were made at an effective gas temperature of 1450° F (at the leading edge), a cooling-air temperature of 450° F, and an engine combustion-gas weight flow of 71.4 pounds per second, as described in the PROCEDURE section. The comparisons of the chordwise temperature distributions shown in figure 10 indicate that the distributions for the two blades were similar in shape, but the strut of the strut-supported blade operated at a much lower temperature level than the shell of the shell-supported blade. For example, at a value of coolant-to-gas weight-flow ratio per blade of 0.03, the temperature of the primary supporting member of the strut-supported blade was at least 190° F cooler than the temperature of the primary supporting member of the shell-supported blade at corresponding chord locations. The chordwise variation of the uncooled blade temperature (fig. 10) is due to the variation in local Mach number along the blade (reference 9).

A comparison of the average relative temperature ratios $1-\phi$ of the main supporting member of these two blades at the engine operating conditions stated in the preceding paragraph is shown in figure 11 for various coolant-to-gas weight-flow ratios per blade. The comparison indicates that the strut of the strut-supported blade operated at a lower temperature level than the shell of the shell-supported blade over the entire range of coolant-to-gas weight-flow ratios per blade, and that, at a given value of relative temperature ratio, the strut-supported blade can be operated at a much lower coolant-to-gas weight-flow ratio per blade than the shell-supported blade.

Stress-ratio factors (for range of coolant flows) of strut-supported blade and shell-supported blade with internal tubes. - In order to determine the relative load-carrying capacity of the strut-supported blade, a comparison was made of the stress-ratio factors of the internal-strut-supported blade and an improved shell-supported blade (blade 12, reference 9) over a range of coolant-to-gas weight-flow ratios per blade. The comparison was made at conditions of rated engine speed (11,500 rpm), effective gas temperature of 1450° F, cooling-air temperature of 450° F, and with the assumption that the two blades were made of a noncritical material, Timken 17-22A(S) alloy steel. The stress-to-rupture curve for 100-hour life used in this comparison is shown in figure 12.

The results of the comparison shown in figure 13 indicate that the stress-ratio factor or the load-carrying capacity of the strut-supported blade is better than that of the improved shell-supported blade below ratios of coolant-to-gas weight-flow ratio per blade of approximately 0.09. The comparison also indicates that the stress-ratio factor of the strut-supported blade is relatively constant because the strut temperature at all coolant flows was low enough (below 900° F) that the allowable stress of the blade was only slightly affected by temperature changes (see fig. 12). However, the stress-ratio factor of the shell-supported blade is affected considerably by coolant flow because the temperature of the shell is in the range (900° to 1100° F) where small temperature changes have a large effect on allowable stresses. The root stress in the shell-supported blade is lower than the root stress in the strut-supported blade, but only at high ratios of coolant-to-gas weight-flow ratios per blade (more than 0.04) can the temperature of the shell of the shell-supported blade be reduced to the point where the lower stress level of the shell-supported blade gives a higher stress-ratio factor for this blade than for the strut-supported blade. At these higher coolant-to-gas weight-flow ratios per blade, the temperature of the strut will still be lower than the temperature of the shell of the shell-supported blade. A comparison of the change in stress-ratio factor with coolant-to-gas weight-flow ratio per blade in figure 13 shows that at a coolant-to-gas weight-flow ratio per blade of 0.04, the stress-ratio factors of the two blades are approximately equal.

but at a coolant-to-gas weight-flow ratio per blade of 0.03, the stress-ratio factor for the strut-supported blade is 3.06 whereas that for the shell-supported blade is 2.51. This difference in stress-ratio factor increases rapidly with a decrease in coolant-to-gas weight-flow ratio per blade. The strut blade, because of this higher stress-ratio factor at low coolant flows, possibly could be operated at higher turbine-inlet temperatures for a given coolant-to-gas weight-flow ratio per blade or at lower coolant-to-gas flow ratios per blade for given turbine-inlet temperatures than the shell-supported blade. Rough calculations indicate that the strut-supported blade made of Timken 17-22A(S) could be operated at an effective gas temperature of approximately 2000° F at a coolant-to-gas weight-flow ratio per blade of 0.035 with the cooling-air temperature of 450° F.

Cooling effectiveness (for range of pressure losses) of strut-supported blade and shell-supported blades. - A comparison of the cooling effectiveness Φ of the strut-supported blade with that of a 15-fin blade (reference 2) and a reverse-flow blade (reference 4) over a range of pressure losses at an engine speed of 10,000 rpm is shown in figure 14. The most significant feature of this figure is that for a given pressure loss the strut-supported blade temperatures are lower at any given chordwise position than the temperature for either of the other two blades (high value of Φ represents a low blade temperature). The coolant flow range for all three blades was approximately the same; therefore, for a given coolant-flow rate the pressure loss for the strut blade is higher than that for the 15-fin blade, but lower than that for the reverse-flow blade.

The magnitude of the chordwise temperature gradients for the three blades is indicated by the spread in the values of Φ between the leading edge and the midchord regions of the blade. Even though the pressure losses for the 15-fin blade were low, the temperature gradients were very high. The film-cooled, reverse-flow blade was designed to minimize the chordwise temperature gradients, but this was accomplished only at the cost of high cooling-air pressure losses. In addition to the high cooling effectiveness, the strut-supported blade had low chordwise temperature gradients of approximately the same magnitude as the reverse-flow blade, but these low temperature gradients were obtained at much lower pressure losses. The pressure losses for the strut-supported blade possibly could be decreased by the proper design of the cooling-air passages within the blade. A brief analysis of the factors that might cause the losses in the strut-supported blade to be higher than those in the 15-fin blade was therefore made in order to obtain some insight for improving future blade designs. A comparison was made of the areas and flow paths through the strut blade and through the 15-fin blade along with a rough calculation of the contraction and expansion losses that occur in the flow paths. This analysis indicated that the flow areas and the friction losses for the two blades are approximately the same for three-fourths of the blade span from the

blade root; but large losses occur in the base and at the 3/4-span section of the strut-supported blade. The losses that occur in the strut-supported blade are: the expansion losses that occur in the base where the air passes through two slots and then expands into the plenum chamber at the platform of the blade (fig. 3(b)), the contraction losses that occur when the air leaves the plenum chamber and enters a much smaller area that is bounded by the shell and strut at the root, and the expansion losses that occur at the 3/4-span position from the root where the flow area suddenly increases because of the termination of the main body of the strut and the 0.020-inch thick fins. Although these pressure losses are caused by turbulence that increases the heat-transfer rate to the cooling air, this turbulence occurs only in local regions where its effect is neither useful nor widespread. From the brief analysis that was made, apparently the pressure losses through the strut-supported blade can be greatly reduced if future designs eliminate or decrease the sudden changes in flow areas within the blade, especially the sudden change in flow area at the plenum chamber at the platform of the blade base. Even with the present design, however, the strut-supported blade cooled more effectively for a given pressure loss than any blade previously investigated.

Comparison of Extrapolated Experimental and

Calculated Average Strut Temperatures

A comparison of average strut temperatures at the 3/8-span section determined from extrapolated experimental data from the present report and values analytically calculated in reference 10 is presented in figure 15. The experimental data were extrapolated to the conditions of the calculated data ($T_{g,e}$ of 1530° F and $T_{a,e,h}$ of 200° F) by use of the average values of $1-\phi$ from figure 11. The calculated data shown in figure 15 were taken from figure 7 of reference 10. From figure 15 apparently the experimental and the calculated data agree fairly well over the range covered by the comparison. Up to a coolant-to-gas weight-flow ratio per blade of 0.02, the maximum difference between the extrapolated measured and the calculated temperatures amounts to about 60° F, which is less than 10 percent of the strut temperature. An inspection of figure 12 shows that this 60° F variation will have very little effect on the allowable strength of Timken 17-22A(S) below about 900° F, but will have a decided effect on the strength for temperatures above 900° F. From this comparison the analytical method of reference 10 is concluded to be sufficiently accurate for predicting the approximate temperature level in a strut-supported blade for design purposes as long as the strut temperatures are below about 900° F.

SUMMARY OF RESULTS

The following results were obtained in an experimental investigation in order to determine the cooling effectiveness and cooling-air pressure losses of an internal-strut-supported air-cooled turbine-rotor blade.

1. The relative temperature ratio (ratio of strut temperature to effective gas temperature when both are corrected by the cooling-air temperature at the blade root) gave an approximate correlation of the strut-temperature data and permitted extrapolation of the data to operating conditions other than the experimental operating conditions.

2. The main support member of the strut-supported blade was much cooler than the shell of the shell-supported blades under the same operating conditions. At rated engine speed with cooling air bled from the compressor discharge and a coolant-to-gas weight-flow ratio per blade of 0.03, the temperatures of the strut over the entire chord at the 3/8-span position were about 190° F below the corresponding temperatures of the shell of the most promising shell-supported blade previously investigated.

3. The strut-supported blade showed greater potential for higher gas-temperature operation than the shell-supported blade, or at current gas temperatures, the strut-supported blade operated at lower coolant-to-gas weight-flow ratios per blade than the shell-supported blade.

4. Below a coolant-to-gas weight-flow ratio per blade of 0.04 at rated engine operating conditions, the stress-ratio factor of the strut-supported blade was higher than that of the shell-supported blade, thus indicating a greater load-carrying capacity for the strut-supported blade at lower cooling-air flows.

5. Cooling-air pressure losses through the strut-supported blade were within the range of losses encountered in shell-supported blades previously investigated. Analysis of the cooling-air passage configurations in the strut blade indicated that these losses could be reduced by redesign of the passages at the blade base without decreasing the cooling effectiveness.

6. Comparisons of the cooling effectiveness of the strut-supported blade with those of two shell-supported blades (a 15-fin blade and a reverse-flow blade) over a range of pressure losses at an engine speed of 10,000 rpm indicated that the average temperature level of the strut-supported blade is lower and the chordwise temperature gradients were less than those of the shell-supported blades.

~~CONFIDENTIAL~~

7. Comparison of extrapolated values of experimentally measured average strut temperatures with analytically calculated values showed that the two values agreed within 10 percent at low cooling-air flows and the analytical method of predicting strut temperatures is therefore suitable for design application.

Lewis Flight Propulsion Laboratory
National Advisory Committee for Aeronautics
Cleveland, Ohio

2501

~~CONFIDENTIAL~~

APPENDIX A

METHOD OF ANALYZING SHEAR FORCES IN SPOT WELDS

ATTACHING SHELL TO STRUT

In the calculation of the shear forces in a spot weld between the shell and strut of the internal-strut-supported blade, a 0.27-inch radial spacing between adjacent rows of welds was assumed. This resulted in 14 chordwise rows of spot welds (fig. 2(b)). The calculations of the two loads, centrifugal and thermal, on the spot welds were made separately and then superimposed. There would be some differential elongation between the strut and shell due to centrifugal load alone, but this load was omitted from the calculation of the spot-weld forces because its magnitude would be slight compared with the thermal expansion.

The calculation of the thermal loads on the spot welds was based on the following assumptions:

- (1) The elongation of the shell is equal to that of the strut at each row of spot welds.
- (2) The spot welds supply whatever force is necessary to make up the difference that would occur in elongation between the strut and the shell due to thermal gradient alone if the two were not attached.
- (3) The strut temperature at each station is the average strut temperature at that station. The values used for both average strut temperature and shell temperature were those calculated in reference 10.

An equation for the elongation at any station n (fig. 2(b)) on the shell due to thermal-expansion spot-weld forces is:

$$\delta_{sh,n} = \delta_{sh,n-1} + l\alpha_{sh}\Delta T_{sh} - \frac{(F_n + F_{n+1} + \dots + F_{14})l}{A_{sh}E_{sh}} \quad (B1)$$

A similar equation can be written for the elongation of the strut at station n :

$$\delta_{st,n} = \delta_{st,n-1} + l\alpha_{st}\Delta T_{st} + \frac{(F_n + F_{n+1} + \dots + F_{14})l}{A_{st}E_{st}} \quad (B2)$$

Because the elongation of the shell is assumed to be equal to the elongation of the strut at any station n , equation (B1) can be set equal to equation (B2).

$$\delta_{sh,n-1} + l\alpha_{sh}\Delta T_{sh} - \frac{(F_n + F_{n+1} + \dots + F_{14})l}{A_{sh}E_{sh}} =$$

$$\delta_{st,n-1} + l\alpha_{st}\Delta T_{st} + \frac{(F_n + F_{n+1} + \dots + F_{14})l}{A_{st}E_{st}} \quad (B3)$$

But $\delta_{sh,n-1}$ equals $\delta_{st,n-1}$, therefore these quantities may be eliminated to give

$$(F_n + F_{n+1} + \dots + F_{14}) = \frac{A_{sh}E_{sh}A_{st}E_{st}(\alpha_{sh}\Delta T_{sh} - \alpha_{st}\Delta T_{st})}{A_{sh}E_{sh} + A_{st}E_{st}} \quad (B4)$$

If X_n is set equal to the summation $(F_n + F_{n+1} + \dots + F_{14})$ in each case, 14 equations are obtained, each of which contains one unknown X_n . After solving for this unknown in each case, F_n may be obtained from the equation $F_n = X_n - X_{n-1}$.

APPENDIX B

SYMBOLS

The following symbols are used in this report:

- A cross-sectional area at plane midway between stations n and $n-1$, sq in.
- E elastic modulus of material at plane midway between stations n and $n-1$, lb/sq in.
- F force exerted by row of spot welds in the radial direction, lb
- l radial distance between rows of spot welds at stations n and $n-1$, in.
- N engine speed, rpm
- p static pressure, in. Hg absolute
- p' total pressure, in. Hg absolute
- r radius from center of rotor, ft
- T static temperature, $^{\circ}\text{F}$
- T' total temperature, $^{\circ}\text{F}$
- ΔT temperature increment above 70°F at plane midway between stations n and $n-1$, $^{\circ}\text{F}$
- w weight-flow rate, lb/sec
- X summation of forces F from n^{th} row to tip of blade, lb
- Y pressure-loss parameter, rotor hub to blade tip, in. Hg
- Y_1 pressure-loss parameter, blade root to blade tip, in. Hg
- α average coefficient of thermal expansion between 70°F and temperature at plane midway between stations n and $n-1$, in./in. ($^{\circ}\text{F}$)
- δ change in radial position of any plane when temperature of blade changes from 70°F to assumed operating temperature, in.

- η efficiency of cooling-air compression in turbine rotor
- ρ density, slug/cu ft
- φ temperature-difference ratio, $(T_{g,e} - T_B)/(T_{g,e} - T_{a,e,h})$
- ω angular velocity of rotor, radians/sec

Subscripts:

- A combustion air
- a blade-cooling air
- B cooled-blade primary support member
- c compressor
- e effective temperature
- g combustion gas
- H hub of rotor
- h root of blade
- i inlet
- m mixture of combustion gas and of scavenge, bearing-cooling, and blade-cooling air in tail pipe
- n n^{th} station (fig. 2(b))
- n-1 $(n-1)^{\text{st}}$ station (fig. 2(b))
- r rotating conditions
- s static conditions
- sh blade shell
- st blade strut
- T blade tip
- O NACA standard sea-level conditions

REFERENCES

1. Ellerbrock, Herman H., Jr., and Stepka, Francis S.: Experimental Investigation of Air-Cooled Turbine Blades in Turbojet Engine. I - Rotor Blades with 10 Tubes in Cooling-Air Passages. NACA RM E50I04, 1950.
2. Hickel, Robert O., and Ellerbrock, Herman H., Jr.: Experimental Investigation of Air-Cooled Turbine Blades in Turbojet Engine. II - Rotor Blades with 15 Fins in Cooling-Air Passages. NACA RM E50I14, 1950.
3. Hickel, Robert O., and Smith, Gordon T.: Experimental Investigation of Air-Cooled Turbine Blades in Turbojet Engine. III - Rotor Blades with 34 Steel Tubes in Cooling-Air Passages. NACA RM E50J06, 1950.
4. Ellerbrock, Herman H., Jr., Zalabak, Charles F., and Smith, Gordon T.: Experimental Investigation of Air-Cooled Turbine Blades in Turbojet Engine. IV - Effects of Special Leading- and Trailing-Edge Modifications on Blade Temperature. NACA RM E51A19, 1951.
5. Smith, Gordon T., and Hickel, Robert O.: Experimental Investigation of Air-Cooled Turbine Blades in Turbojet Engine. V - Rotor Blades with Split Trailing Edges. NACA RM E51A22, 1951.
6. Arne, Vernon L., and Esgar, Jack B.: Experimental Investigation of Air-Cooled Turbine Blades in Turbojet Engine. VI - Conduction and Film Cooling of Leading and Trailing Edges of Rotor Blades. NACA RM E51C29, 1951.
7. Smith, Gordon T., and Hickel, Robert O.: Experimental Investigation of Air-Cooled Turbine Blades in Turbojet Engine. VIII - Rotor Blades with Capped Leading Edges. NACA RM E51H14, 1951.
8. Stepka, Francis S., and Hickel, Robert O.: Experimental Investigation of Air-Cooled Turbine Blades in Turbojet Engine. IX - Evaluation of the Durability of Noncritical Rotor Blades in Engine Operation. NACA RM E51J10, 1951.
9. Esgar, Jack B., and Clure, John L.: Experimental Investigation of Air-Cooled Turbine Blades in Turbojet Engine. X - Endurance Evaluation of Several Tube-Filled Rotor Blades. NACA RM E52B13.
10. Schramm, Wilson B., and Nachtigall, Alfred J.: Analysis of Coolant-Flow Requirements for an Improved, Internal-Strut-Supported, Air-Cooled Turbine-Rotor Blade. NACA RM E51L13, 1952.

11. Long, Roger A., and Esgar, Jack B.: Experimental Investigation of Air-Cooled Turbine Blades in Turbojet Engine. VII - Rotor-Blade Fabrication Procedures. NACA RM E51E23, 1951.
12. Anon.: Timken 17-22A and Other Bolting Steels for High Temperature Applications. Tech. Bull. No. 36, Timken Bolting Steel Data Sheets, Steel and Tube Div., The Timken Roller Bearing Company (Canton), 1949.

TABLE I - SUMMARY OF ENGINE OPERATING CONDITIONS WITH FULL-LENGTH BLADE

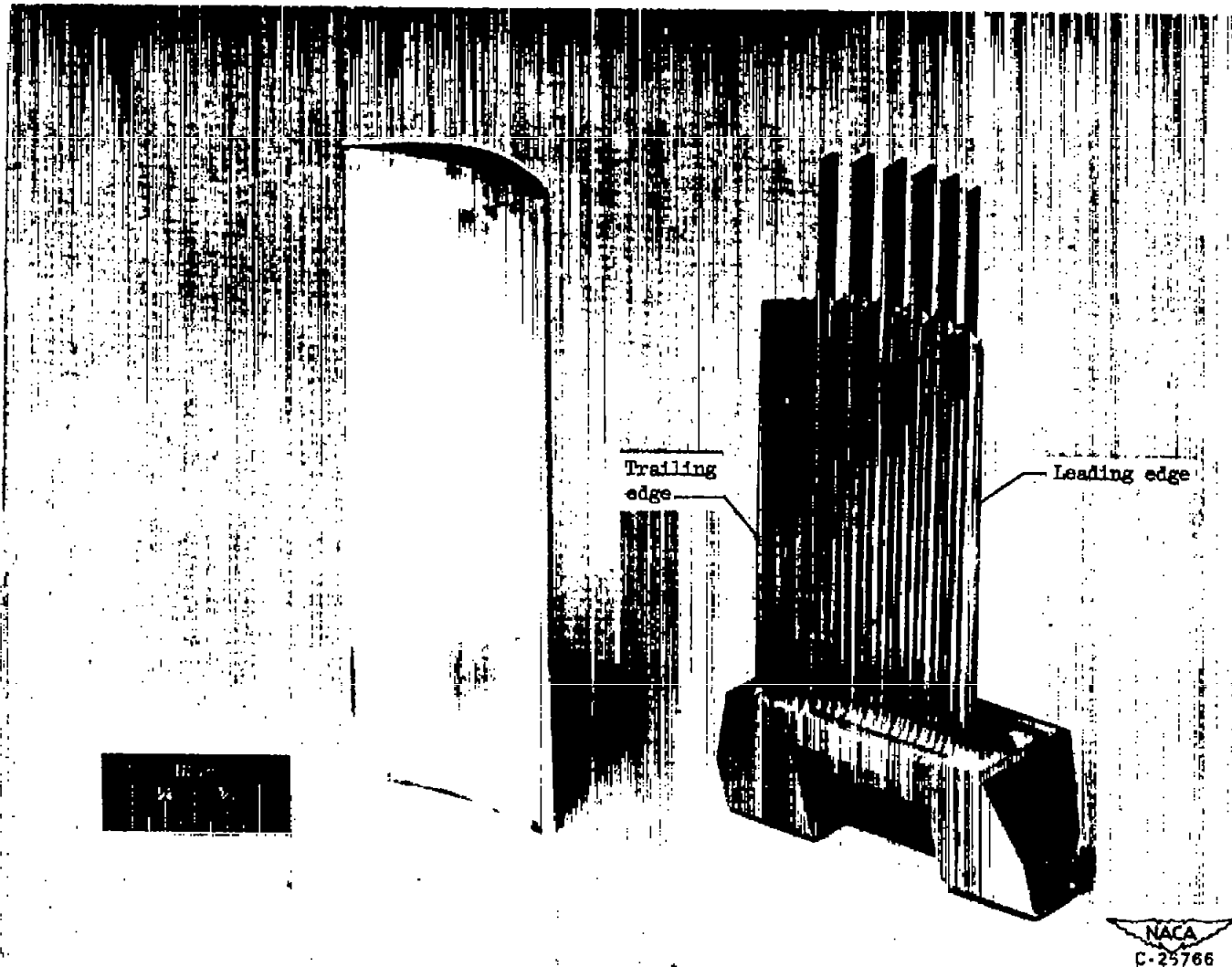


Series	Engine speed N (rpm)	Average effective gas temperature $T_{g,e}$ (°F)	Average conditions at compressor inlet		Cooling-air weight flow per blade w_a (lb/sec)	Coolant-to- gas weight- flow ratio per blade w_a/w_g	Relative temperature ratio 1 - ϕ			
			Total pressure $P_{A,c,i}$ (in. Hg abs)	Total temperature $T_{A,c,i}$ (°F)			Thermocouple location			
							3	4	5	6
A	4008	1138	29.84	87.9	0.050	0.138	0.198	0.285	0.135	0.179
	4000				.040	.110	.231	.315	.159	.207
	3998				.036	.099	.247	.325	.171	.220
	4006				.031	.085	.274	.351	.190	.238
	4006				.025	.069	.281	.374	.215	.262
	4002				.020	.055	.288	.400	.242	.284
	3996				.015	.041	.352	.436	.277	.318
	4008				.012	.033	.380	.465	.301	.337
	4010				.010	.028	.413	.494	.330	.363
B	6008	1066	28.83	80.9	0.051	0.097	0.224	0.323	0.181	0.219
	6006				.041	.078	.257	.357	.205	.248
	6012				.036	.068	.272	.371	.218	.257
	6014				.031	.059	.296	.397	.237	.279
	6008				.026	.049	.320	.419	.257	.297
	5998				.020	.038	.355	.454	.286	.327
	6006				.015	.029	.396	.492	.324	.355
	5996				.013	.025	.426	.522	.359	.382
	5996				.010	.019	.465	.558	.398	.408
C	8060	1041	29.29	84.9	0.079	0.103	0.199	0.289	0.177	0.202
	8080				.072	.094	.210	.307	.188	.219
	7996				.063	.083	.223	.326	.200	.233
	7990				.051	.067	.243	.348	.218	.250
	8052				.040	.052	.279	.378	.238	.279
	8022				.036	.047	.290	.391	.248	.292
	8020				.031	.041	.310	.408	.263	.302
	8022				.025	.033	.333	.433	.282	.319
D	9028	1065	29.29	86.8	0.094	0.106	0.191	0.284	0.176	0.204
	8980				.079	.089	.211	.306	.189	.226
	9064				.071	.080	.227	.325	.205	.239
	9018				.064	.072	.245	.341	.215	.255
	8994				.051	.058	.257	.355	.223	.265
	9000				.040	.045	.284	.385	.243	.284
	9006				.036	.041	.302	.400	.260	.300
	9018				.030	.034	.320	.417	.271	.313
	9008				.025	.028	.340	.438	.287	.329
E	10018	1092	29.29	89.8	0.107	0.104	0.188	0.272	0.180	0.207
	10024				.099	.096	.194	.276	.184	.214
	10026				.095	.091	.199	.292	.189	.218
	10028				.080	.077	.216	.321	.205	.240
	10030				.071	.068	.230	.345	.208	.250
	10050				.063	.061	.248	.369	.224	.267
	10050				.051	.049	.264	.382	.234	.281
	10052				.041	.039	.295	.421	.253	.299
	10046				.035	.034	.300	.437	.258	.310
	10040				.030	.029	.318	.463	.271	.319
	10040				.025	.024	.349	.485	.293	.327

TABLE II - SUMMARY OF ENGINE OPERATING CONDITIONS WITH SHORTENED BLADE

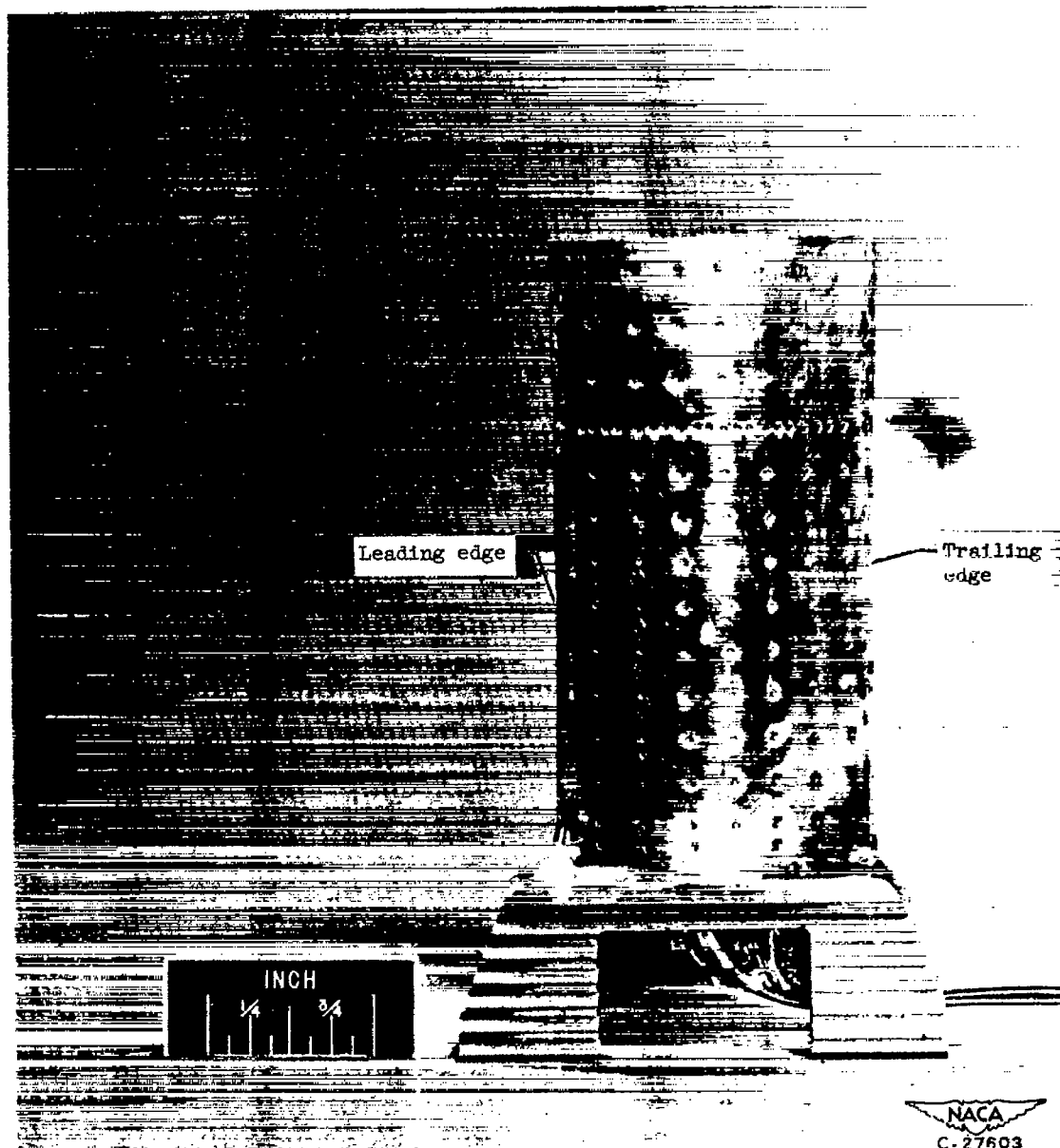


Series	Engine speed N (rpm)	Average effective gas temperature $T_{g,e}$ (°F)	Average conditions at compressor inlet		Cooling-air weight flow per blade w_a (lb/sec)	Coolant-to- gas weight- flow ratio per blade w_a/w_g	Relative temperature ratio 1 - ϕ		
			Total pressure $P'_{A,c,i}$ (in. Hg abs)	Total temper- ature $T'_{A,c,i}$ (°F)			Thermocouple location		
							4	5	6
F	3932	1078	29.46	72.0	0.072	0.197	0.270	0.148	0.187
	3930				.041	.113	.315	.213	.258
	3937				.021	.056	.465	.320	.347
	3937				.010	.028	.535	.396	.400
G	5885	1000	29.47	71.0	0.072	0.136	0.286	0.186	0.225
	5890				.041	.078	.352	.240	.283
	5883				.020	.038	.465	.320	.348
	5880				.010	.020	.524	.376	.388
H	7835	964	29.47	70.0	0.072	0.094	0.343	0.217	0.252
	7845				.050	.066	.379	.247	.281
	7840				.041	.054	.396	.272	.305
	7845				.031	.040	.438	.298	.330
I	9735	1032	29.48	68.0	0.090	0.087	0.327	0.233	0.252
	9740				.071	.069	.376	.262	.282
	9730				.050	.050	.431	.304	.318
	9730				.031	.030	.512	.368	.363
J	11520	1296	29.52	59.0	0.183	0.138	0.277	0.192	0.199
	11498				.160	.121	.284	.192	.210
	11505				.123	.093	.342	.225	.261
	11508				.085	.064	.401	.263	.284
	11503				.064	.048	.453	.304	.312
	11501				.048	.036	.495	.340	.329
	11505				.036	.027	.523	.373	.347
	11501				.024	.018	.575	.459	.367
	11505				.016	.012	.620	.573	.401
	11505				.014	.011	.645	.696	.423



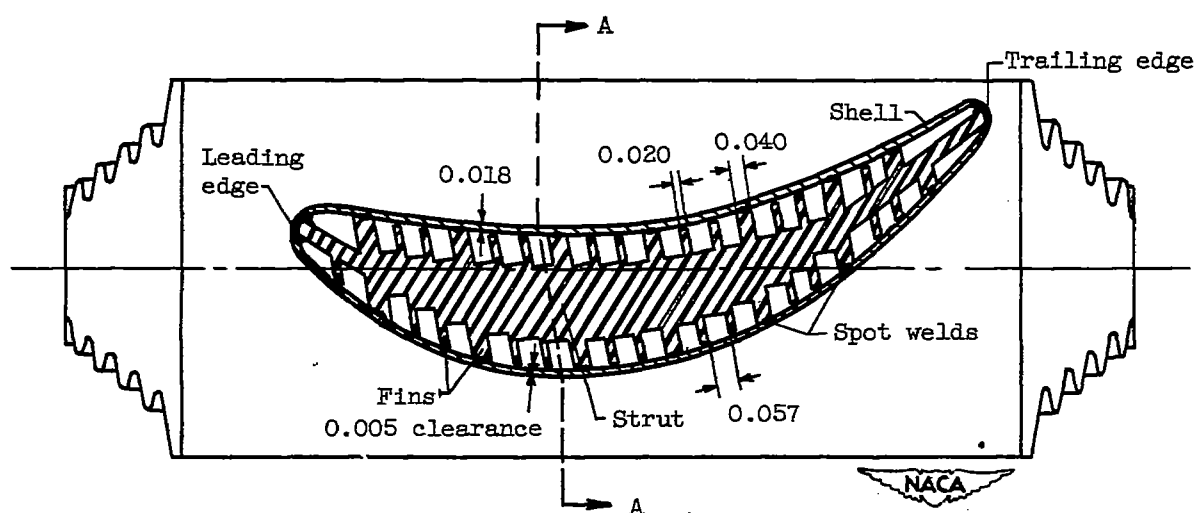
(a) Shell and supporting strut before assembly.

Figure 1. - Internal-strut-supported blade.



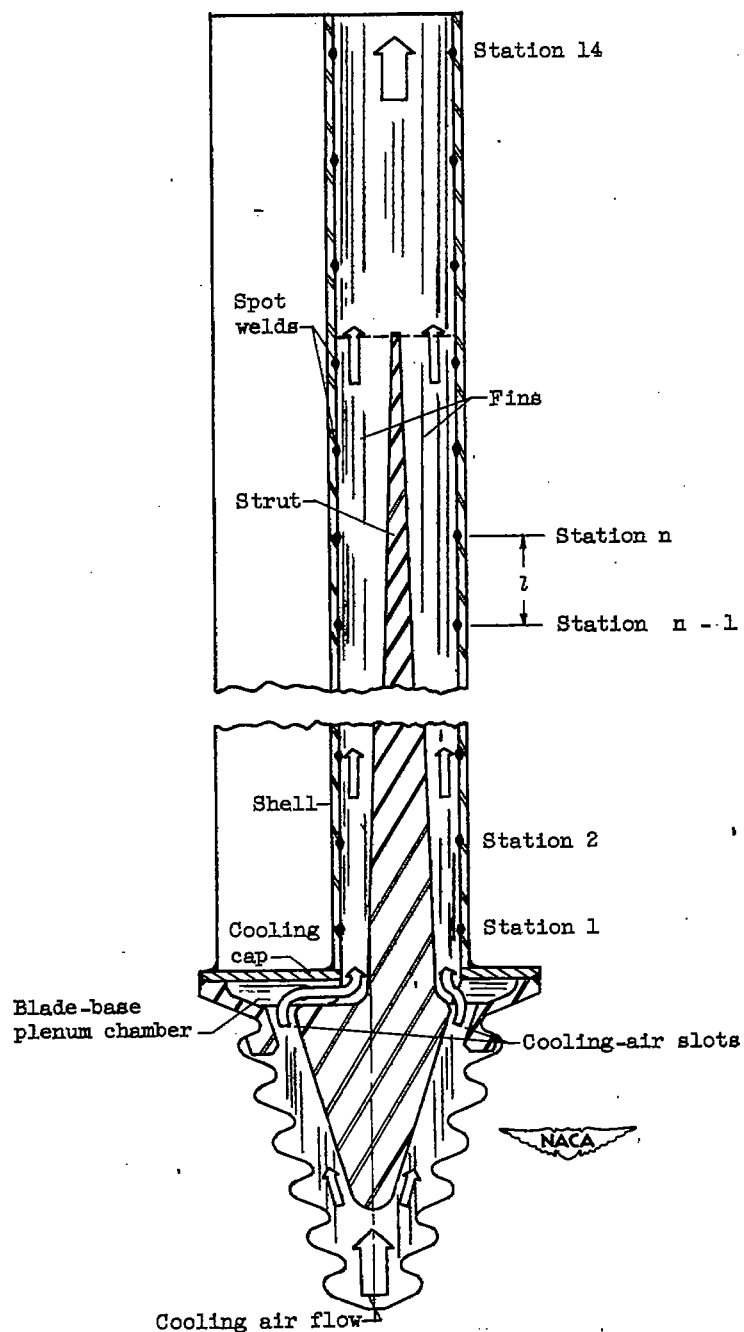
(b) After instrumentation and assembly (suction surface).

Figure 1. - Concluded. Internal-strut-supported blade.



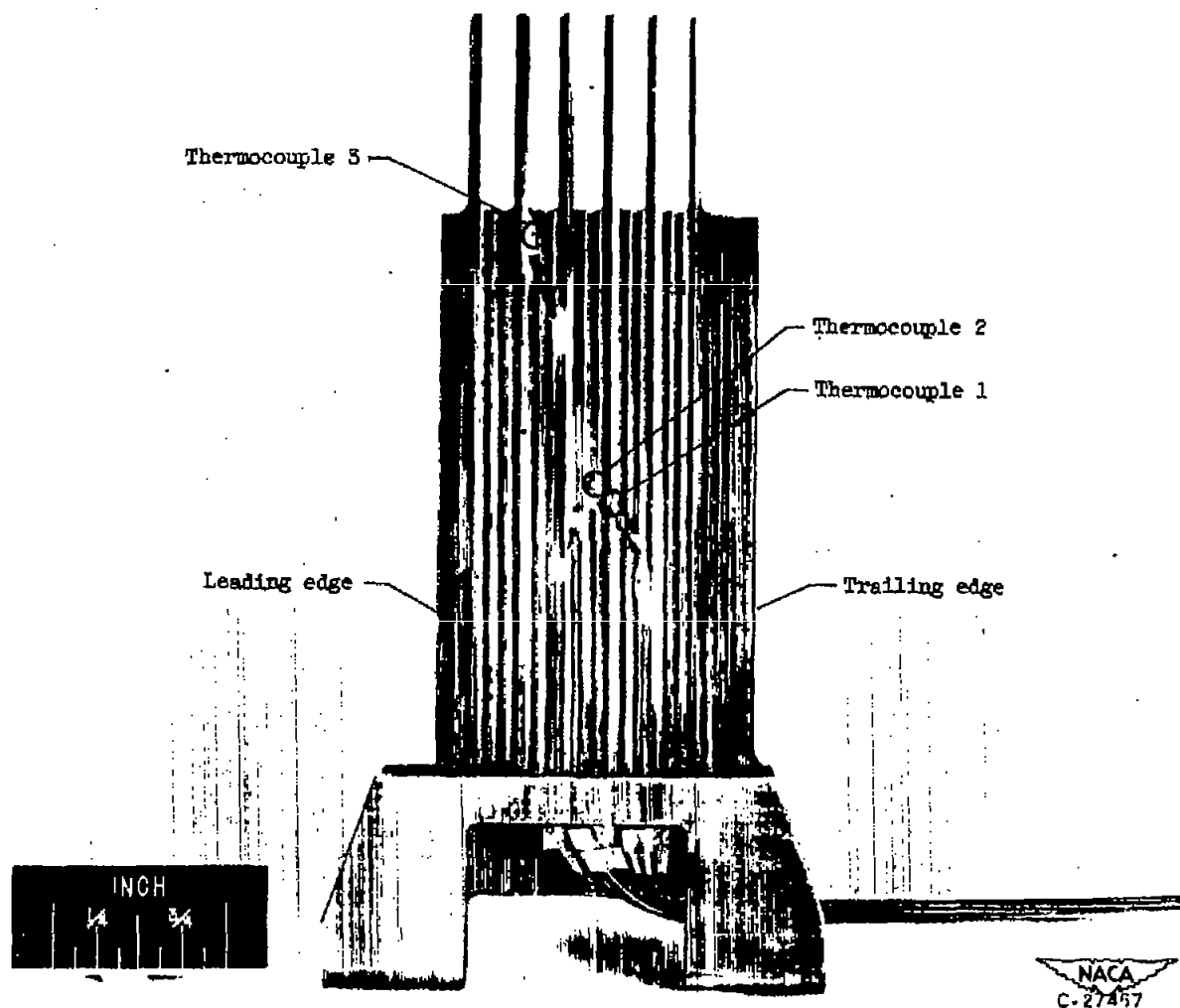
(a) Chordwise cross-sectional view at root section.

Figure 2. - Diagram of air flow passages and spot-weld locations on internal-strut-supported blade. (All dimensions in inches.)



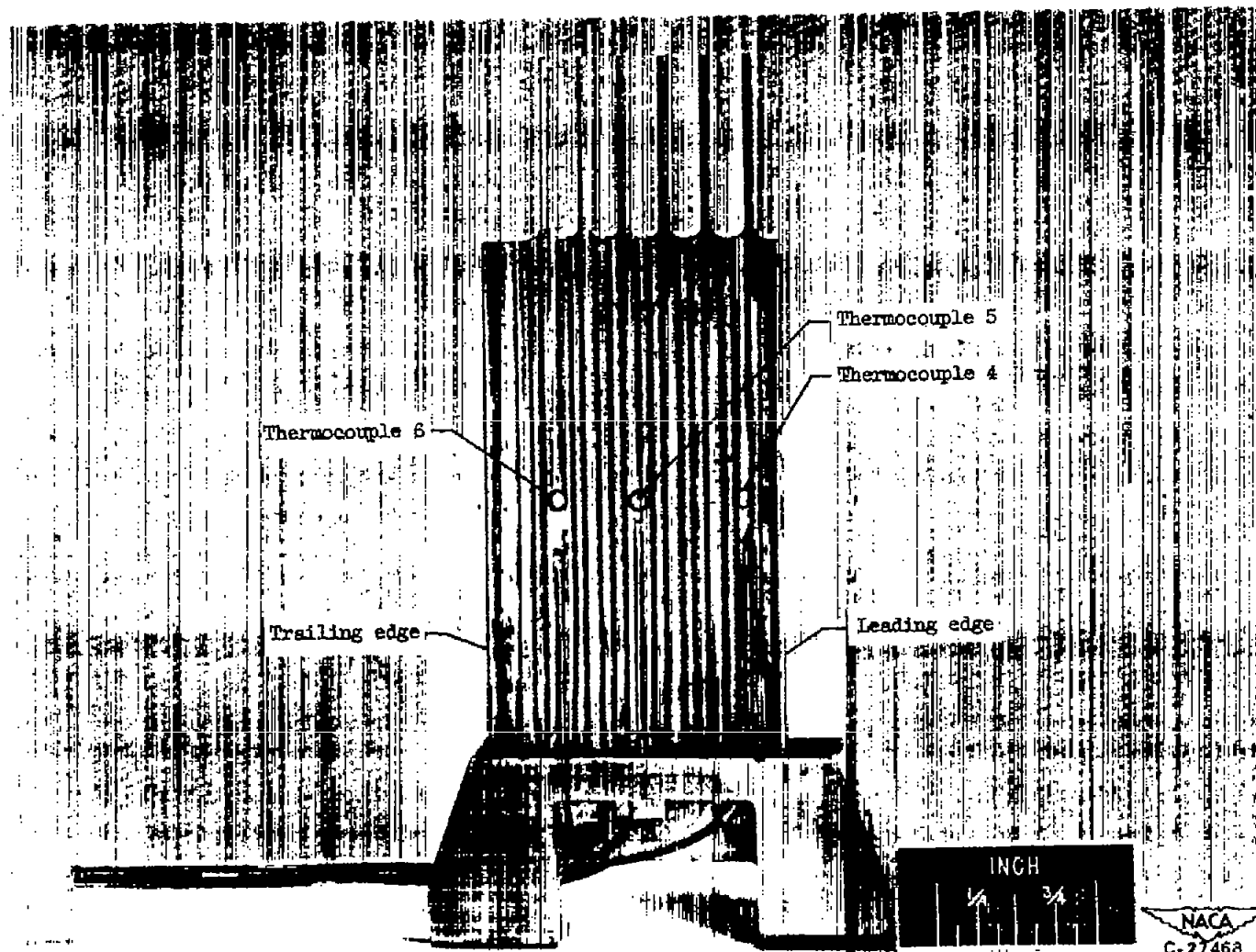
(b) Spanwise cross-sectional view at section A-A.

Figure 2. - Concluded. Diagram of air flow passages and spot-weld locations on internal-strut-supported blade.



(a) Suction surface.

Figure 3. - Thermocouple installations in internal-strut-supported blade.



(b) Pressure surface.

Figure 3. - Concluded. Thermocouple installations in internal-strut-supported blade.

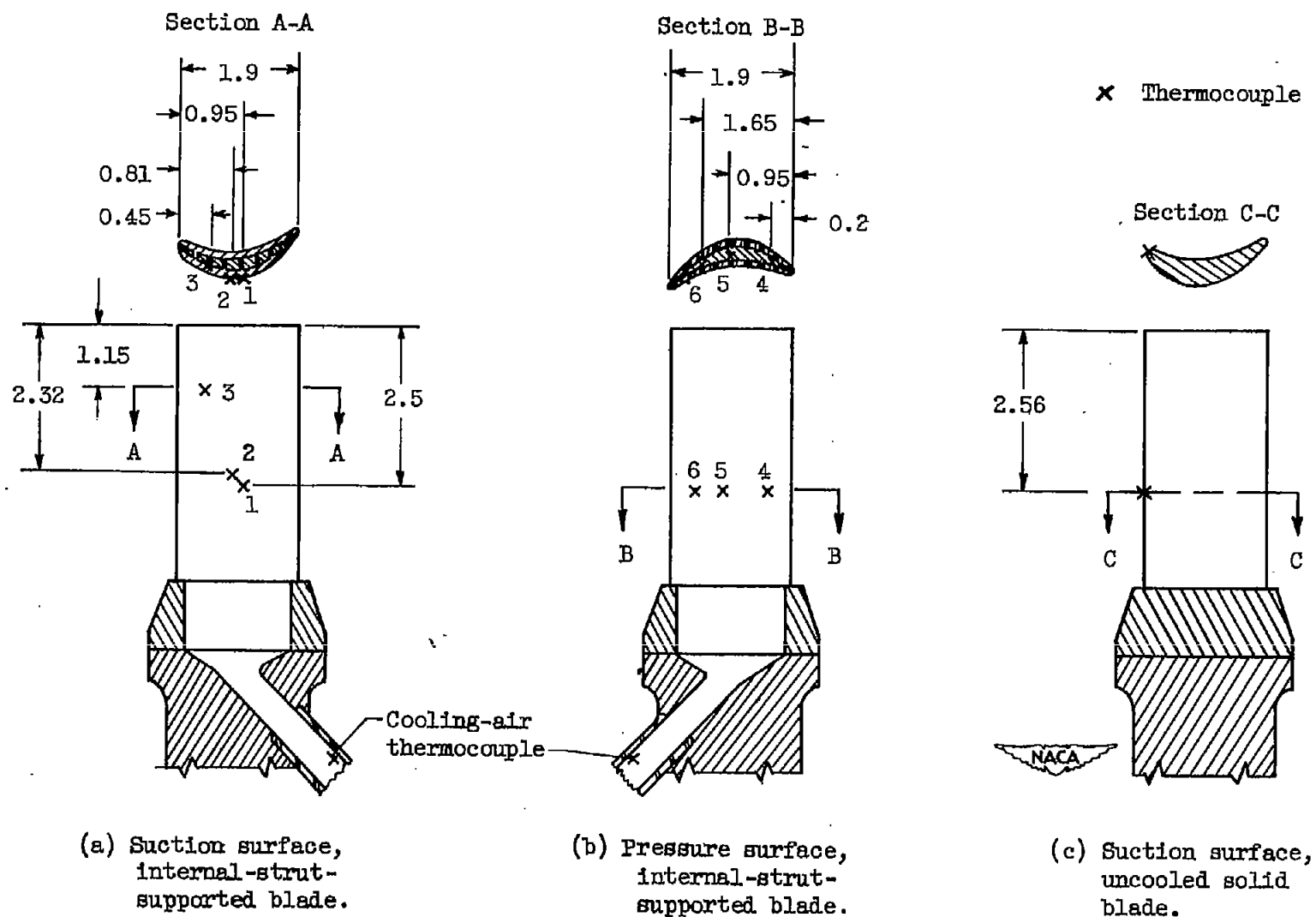


Figure 4. - Schematic diagrams of thermocouple locations on full-length internal-strut-supported blade and uncooled solid blade. (All dimensions in inches.)

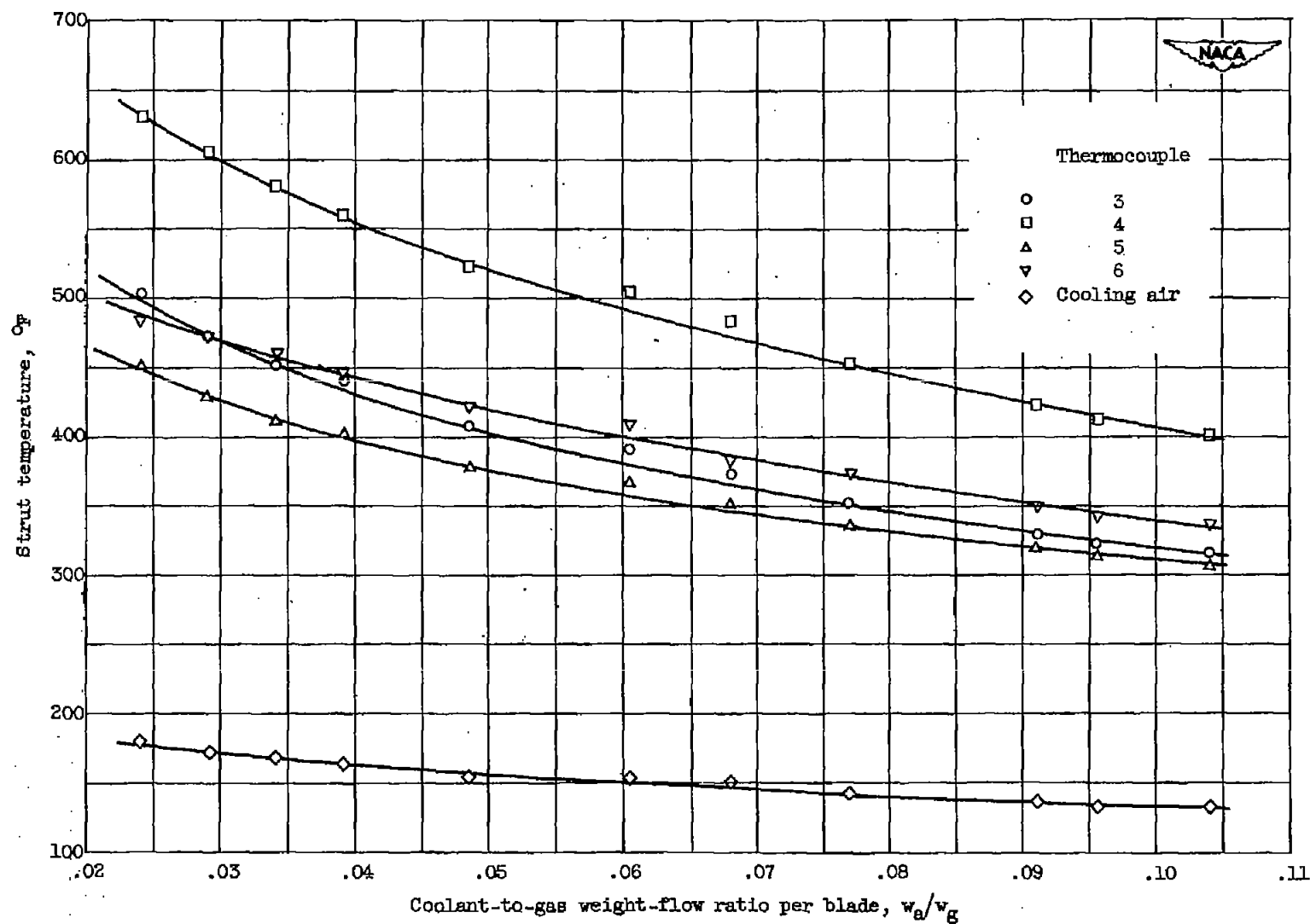


Figure 5. - Variation of strut temperatures on internal-strut-supported blade with coolant-to-gas weight-flow ratio per blade at engine speed of 10,000 rpm and effective gas temperature of 1092° F.

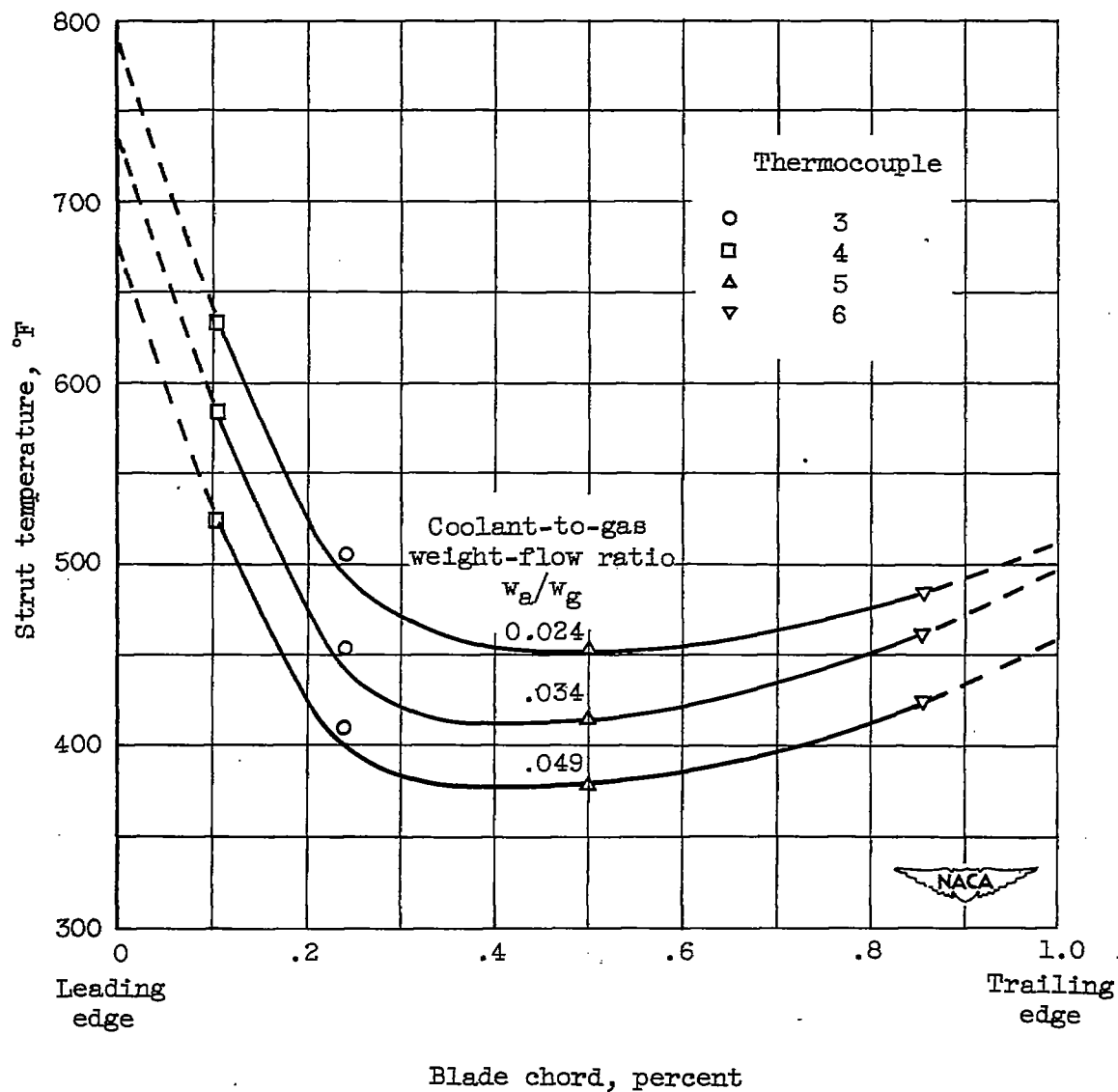


Figure 6. - Chordwise temperature distribution at 3/8-span position on strut of internal-strut-supported blade for various coolant-to-gas weight-flow ratios per blade at engine speed of 10,000 rpm.

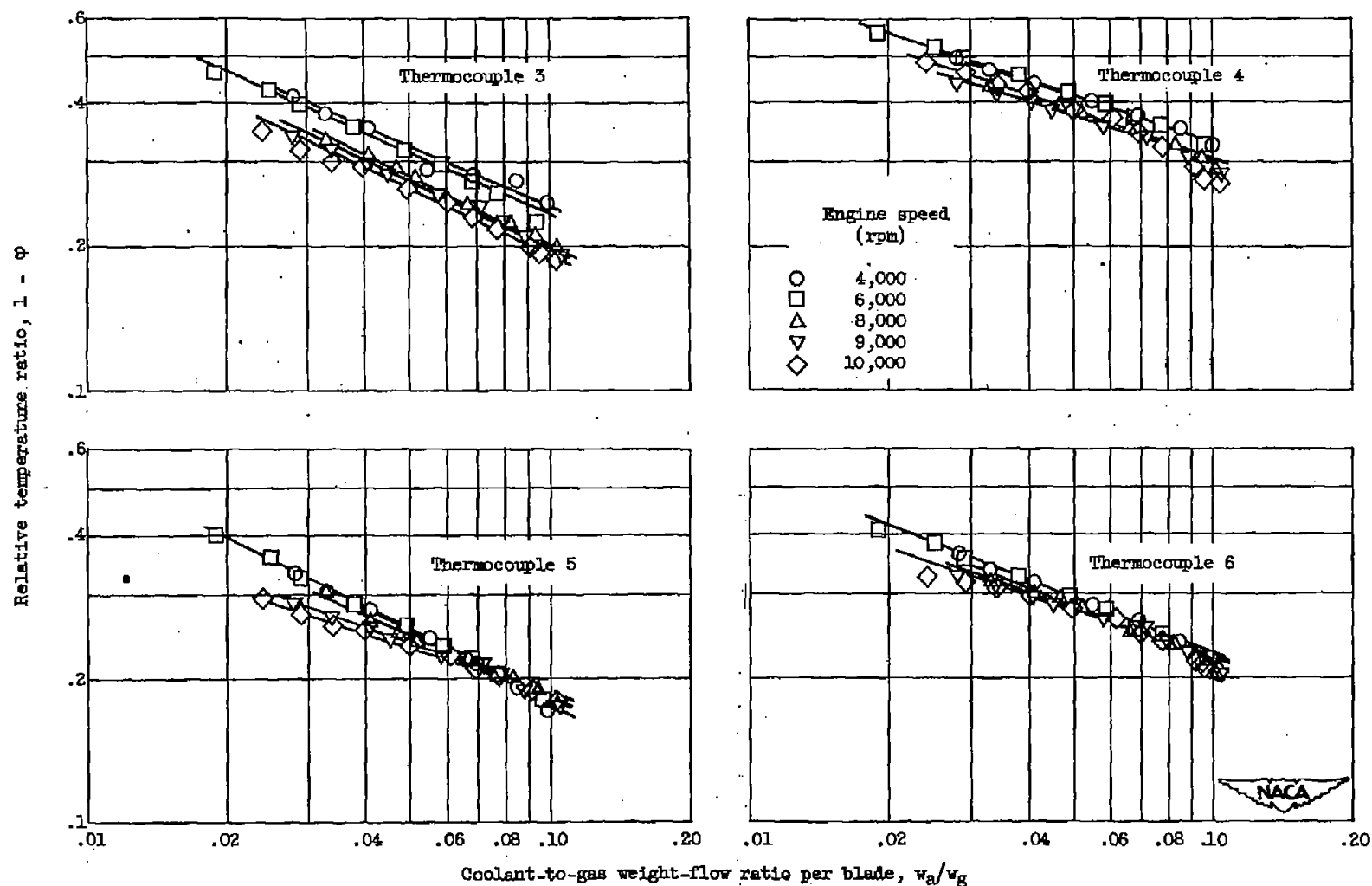


Figure 7. - Variation of relative temperature ratio $1 - \phi$ for strut of internal-strut-supported blade with coolant-to-gas weight-flow ratio per blade over range of engine speeds for thermocouples 3 to 6.

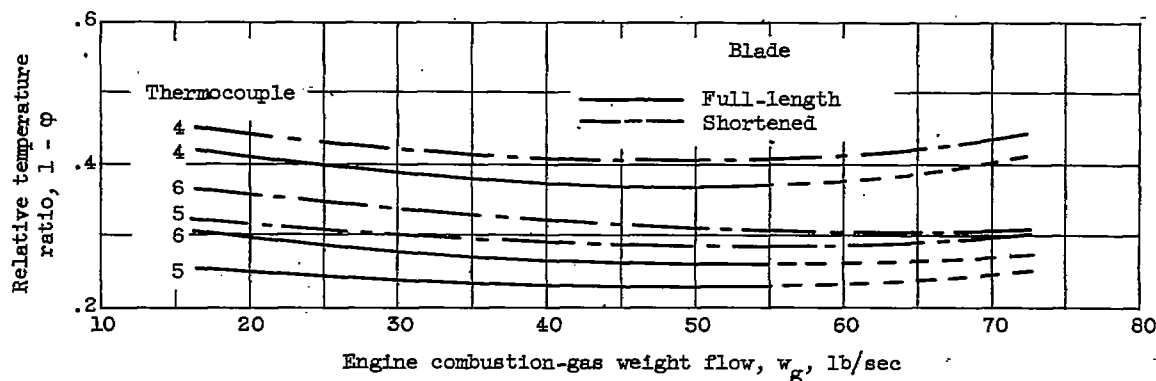


Figure 8. - Variation of relative temperature ratio $1 - \phi$ for struts of full-length and shortened internal-strut-supported blades with engine combustion-gas weight flow for coolant-to-gas weight-flow ratio per blade of 0.05.

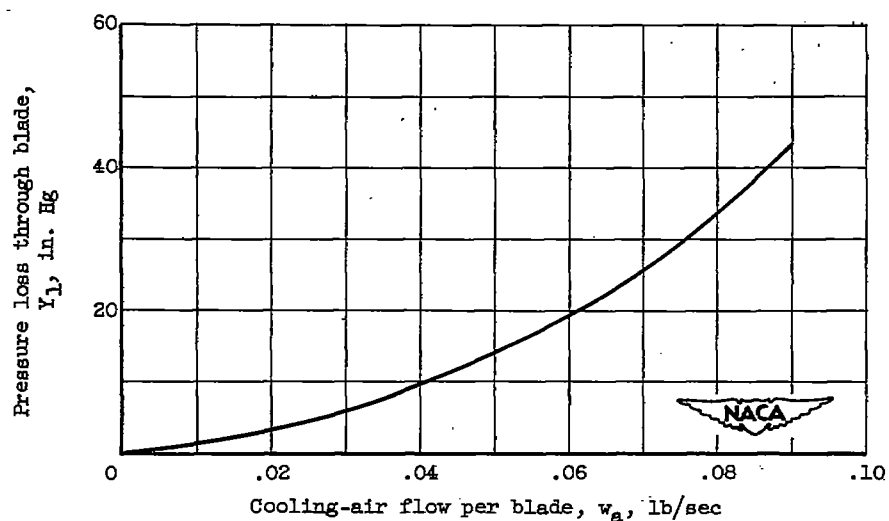


Figure 9. - Cooling-air pressure loss through strut-supported blade for range of cooling-air flows per blade.

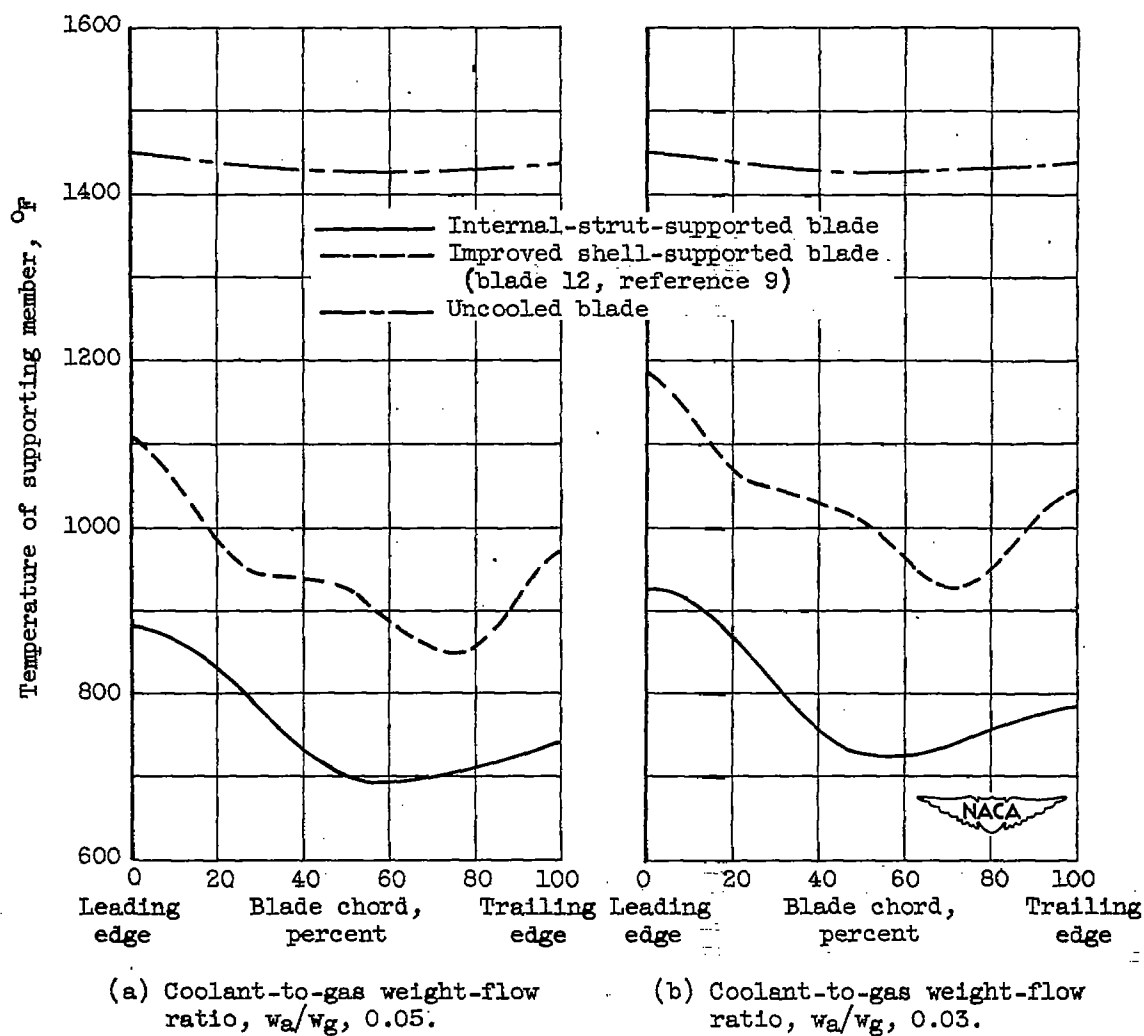


Figure 10. - Comparison of average chordwise temperature distributions of primary supporting member of strut-supported and shell-supported blade at combustion-gas flow of 71.4 pounds per second and engine speed of approximately 11,500 rpm. Cooling-air temperature at blade root, $T_{a,e,h}$, 450°F .

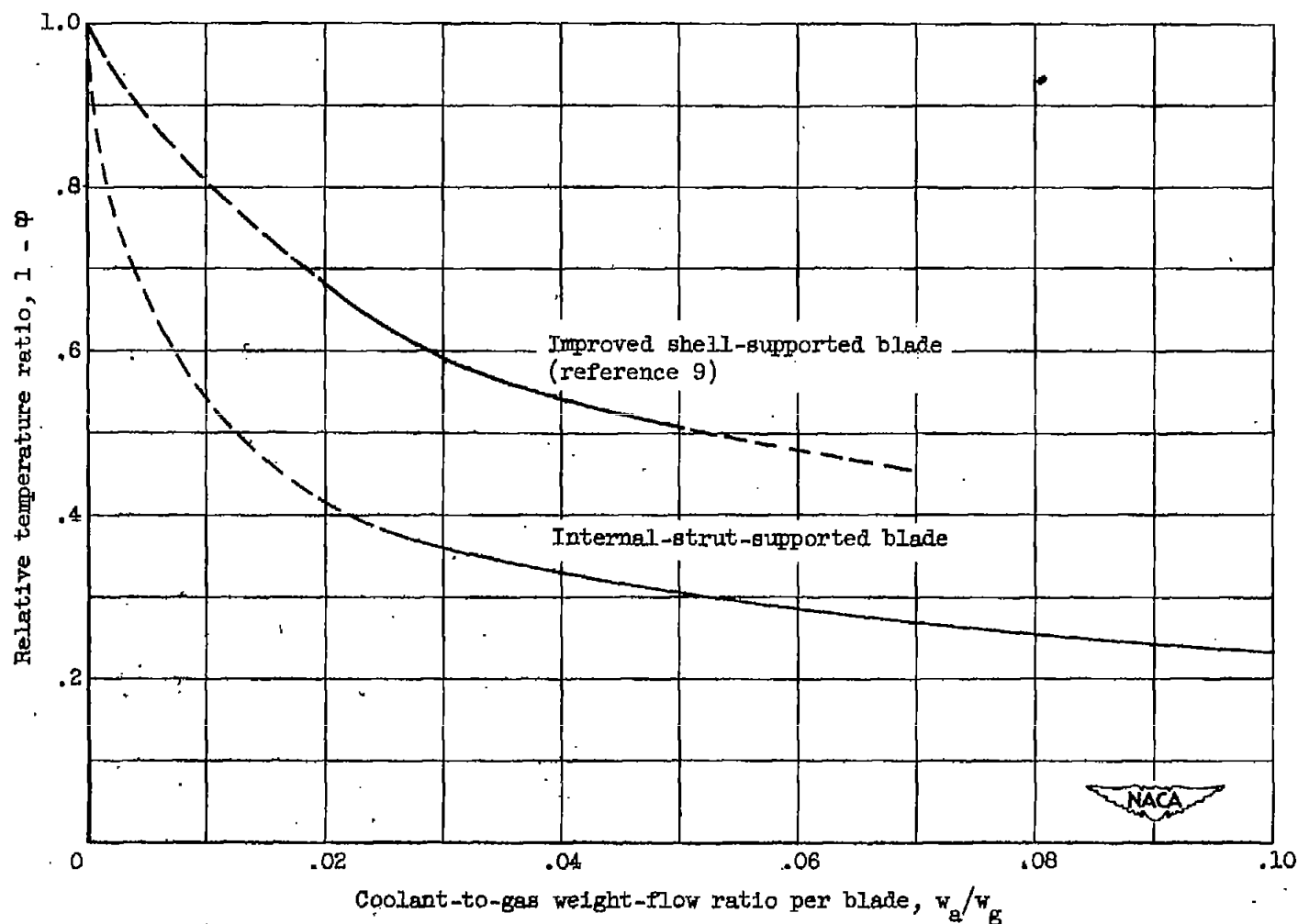


Figure 11. - Comparison of average relative temperature ratios $1 - \phi$ for primary supporting member of improved shell-supported blade and internal-strut-supported blade at 3/8-span position for various coolant-to-gas weight-flow ratios per blade at engine speed of 11,500 rpm.

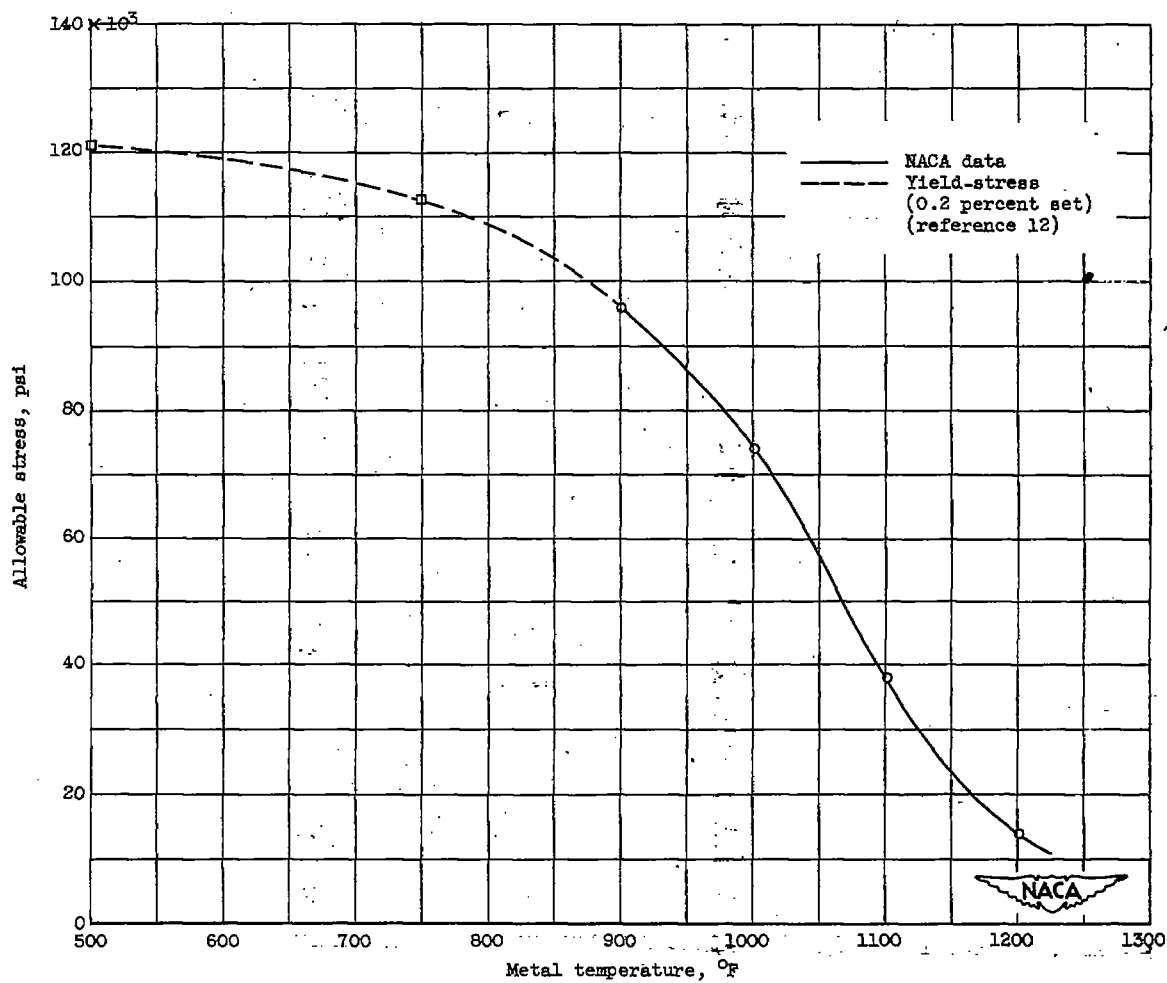


Figure 12. - Stress-rupture data for 100-hour test on Timken 17-22A(6) alloy steel. Heat-treatment: normalized at 1725° F, stress relieved 6 hours at 1200° F and air cooled with a hardness of Rockwell C-34.

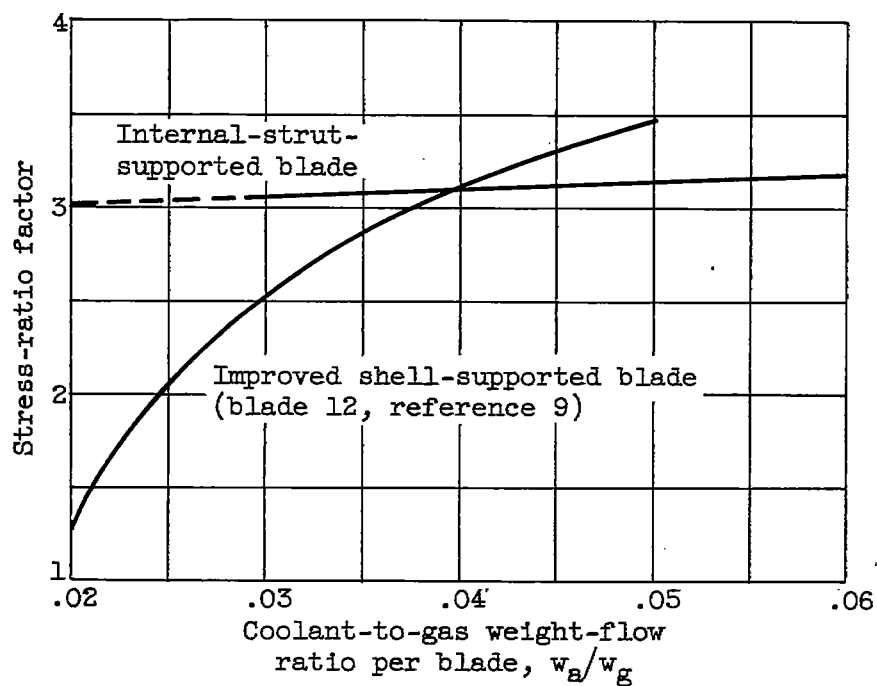


Figure 13. - Comparison of stress-ratio factors of strut-supported blade and shell-supported blade at rated engine speed (11,500 rpm), effective gas temperature of 1450° F, and cooling-air temperature of 450° F.

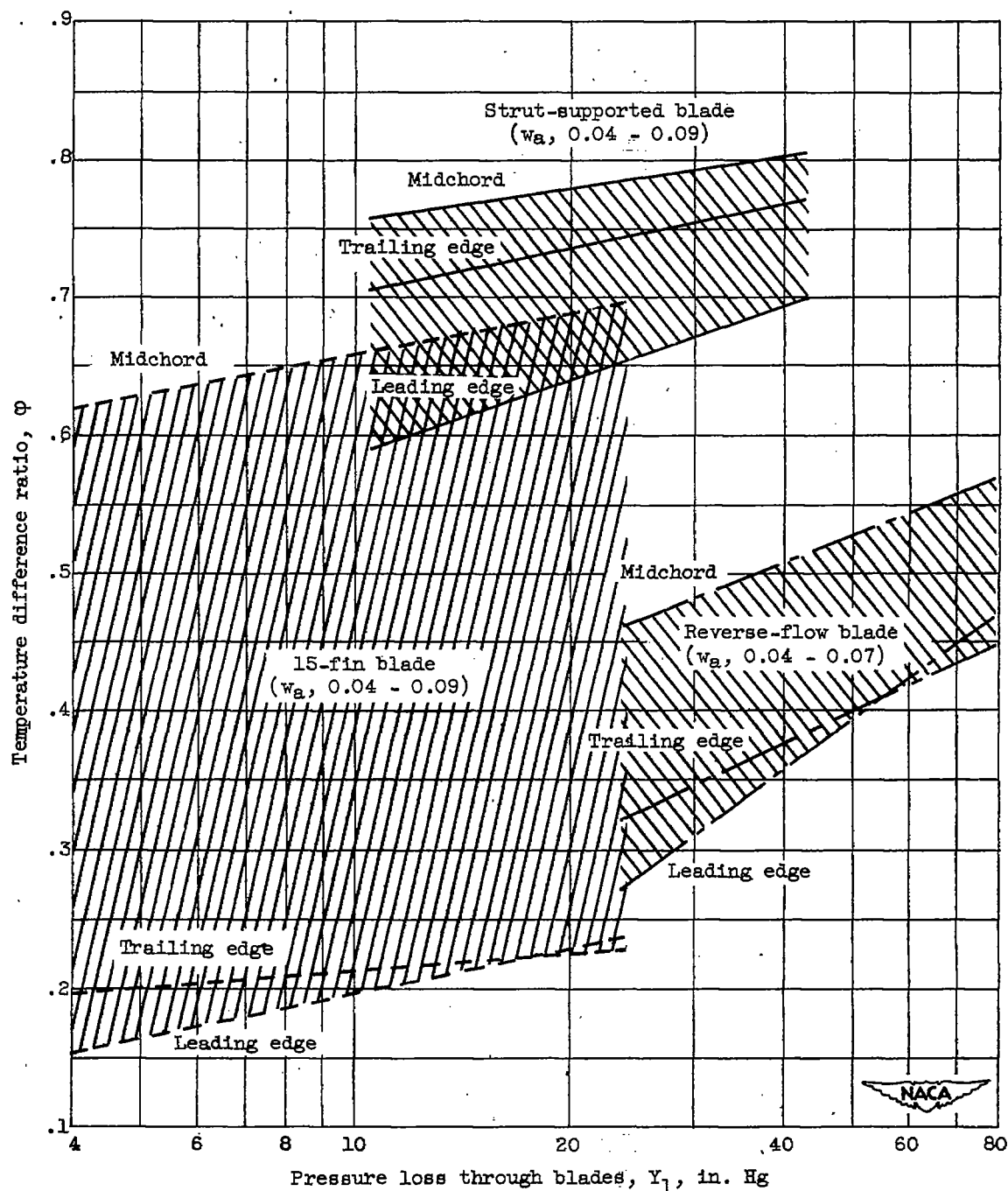


Figure 14. - Comparison of temperature ratio ϕ of several blades over range of cooling-air pressure losses at engine speed of 10,000 rpm. w_a , coolant weight flow.

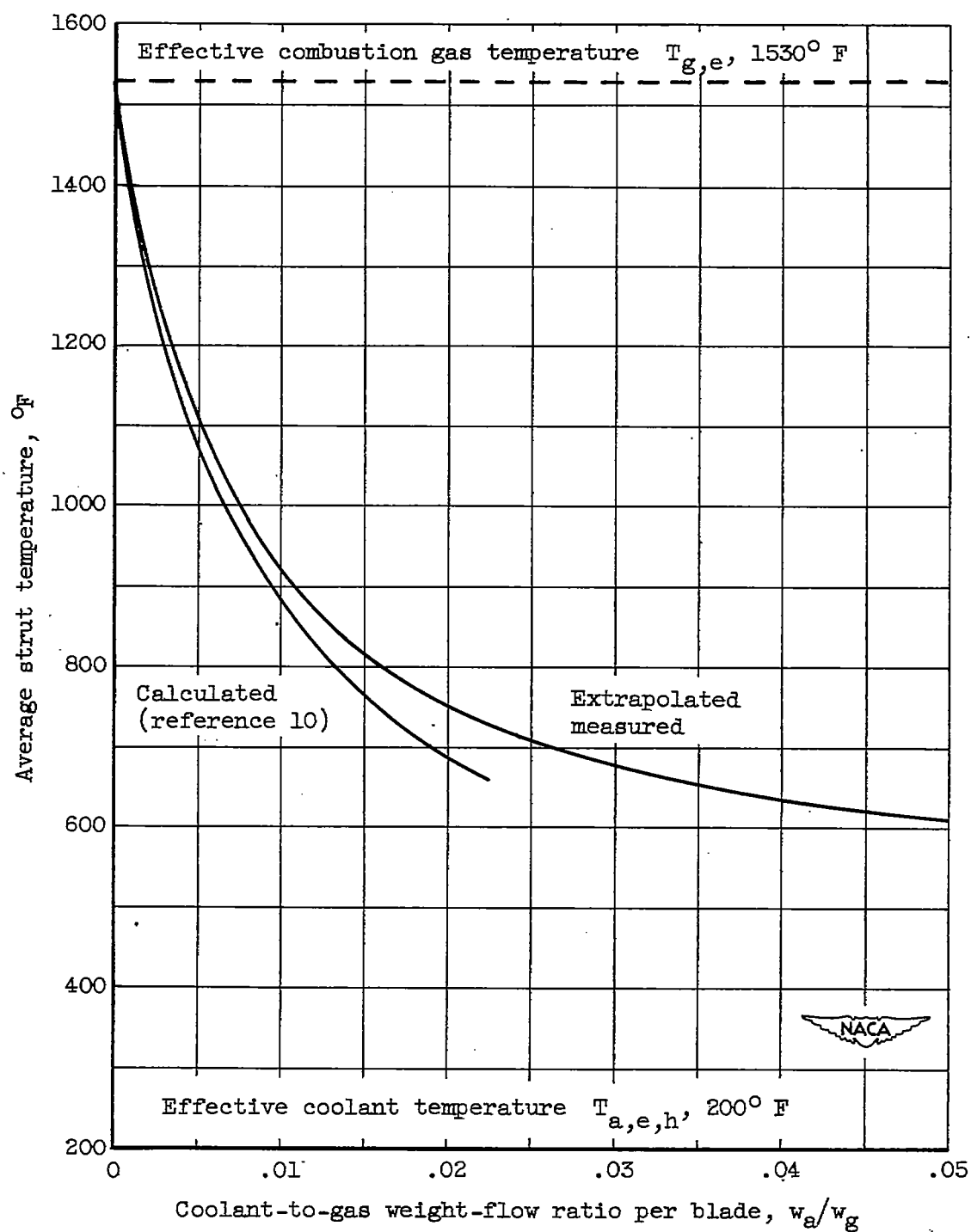


Figure 15. - Comparison of average calculated and measured strut temperatures for various coolant-to-gas weight-flow ratios per blade.